

EVIDENCE FOR A NON-UNIFORM INITIAL MASS FUNCTION IN THE LOCAL UNIVERSE*

GERHARDT R. MEURER¹, O.I. WONG^{2,3}, J.H. KIM¹, D.J. HANISH¹, T.M. HECKMAN¹, J. WERK⁴, J. BLAND-HAWTHORN⁵, M.A. DOPITA⁶, M.A. ZWAAN⁷, B. KORIBALSKI⁸, M. SEIBERT⁹, D.A. THILKER¹, H.C. FERGUSON¹⁰, R.L. WEBSTER³, M.E. PUTMAN¹¹, P.M. KNEZEK¹², M.T. DOYLE¹³, M.J. DRINKWATER¹³, C.G. HOOPES¹, V.A. KILBORN¹⁴, M. MEYER¹⁵, E.V. RYAN-WEBER¹⁶, R.C. SMITH¹⁷, AND L. STAVELEY-SMITH¹⁵

ApJ in press

ABSTRACT

Many of the results in modern astrophysics rest on the notion that the Initial Mass Function (IMF) is universal. Our observations of a sample of H I selected galaxies in the light of H α and the far-ultraviolet (FUV) challenge this result. The extinction corrected flux ratio $F_{\text{H}\alpha}/f_{\text{FUV}}$ from these two tracers of star formation shows strong correlations with the surface-brightness in H α and the R band: Low Surface Brightness (LSB) galaxies have lower $F_{\text{H}\alpha}/f_{\text{FUV}}$ ratios compared to High Surface Brightness (HSB) galaxies as well as compared to expectations from equilibrium models of constant star formation rate (SFR) using commonly favored IMF parameters. Weaker but significant correlations of $F_{\text{H}\alpha}/f_{\text{FUV}}$ with luminosity, rotational velocity and dynamical mass are found as well as a systematic trend with morphology. The correlated variations of $F_{\text{H}\alpha}/f_{\text{FUV}}$ with other global parameters are thus part of the larger family of galaxy scaling relations. The $F_{\text{H}\alpha}/f_{\text{FUV}}$ correlations can not be due to residual extinction correction errors, while systematic variations in the star formation history can not explain the trends with both H α and R surface brightness nor with other global properties. The possibility that LSB galaxies have a higher escape fraction of ionizing photons seems inconsistent with their high gas fraction, and observations of color-magnitude diagrams of a few systems which indicate a real deficit of O stars. The most plausible explanation for the correlations is the systematic variations of the upper mass limit \mathcal{M}_u and/or the slope γ which define the upper end of the IMF. We outline a scenario of pressure driving the correlations by setting the efficiency of the formation of the dense star clusters where the highest mass stars preferentially form. Our results imply that the star formation rate measured in a galaxy is highly sensitive to the tracer used in the measurement. A non-universal IMF would also call into question interpretation of metal abundance patterns in dwarf galaxies as well star formation histories derived from color magnitude diagrams.

Subject headings: galaxies: stellar content – stars: luminosity function, mass function – stars: formation – galaxies: ISM

1. INTRODUCTION

A key concept in our understanding of the evolution of galaxies is the Initial Mass Function (IMF), which gives the statistical distribution of masses of stars that form in a single event. Typically the IMF is parametrized as a power law, or a series of broken power-laws, in stellar mass, \mathcal{M}_* , where the key parameters are the power-law index γ and the lower and upper mass limits to the stars formed \mathcal{M}_l and \mathcal{M}_u respectively. The IMF is crucial in interpreting the nature of galaxies because the light we observe is dominated by the highest mass stars while the total mass in stars is dominated by the lower mass stars. If we know the IMF of a stellar population, and its age, then we can estimate its mass from photometry. Similarly when looking at tracers of star formation, such as H α or ultraviolet (UV) emission, the IMF allows us to convert from luminosity to a star formation rate (SFR).

The crucial assumption underpinning much of the use of the IMF is that it is universal (Gilmore 2001); it does not vary within galaxies or between galaxies. This certainly seems to be the case for star clusters (Kroupa 2001, 2002). Since most star formation occurs in star clusters (Lada & Lada 2003) a universal IMF seems plausible, and is well accepted in the literature.

In recent years there has been accumulating evidence that the IMF is not universal (see review of Elmegreen 2008a). This sets the stage for our study in which we challenge the notion that the upper end of the IMF is uniform using measurements of the integrated H α and UV emission in a sample of H I selected galaxies from the Survey of Ionization in

* Based on observations made with the NASA Galaxy Evolution Explorer. GALEX is operated for NASA by the California Institute of Technology under NASA contract NAS5-98034.

¹ Department of Physics and Astronomy, The Johns Hopkins University, 3400 North Charles Street, Baltimore, MD 21218; meurer@pha.jhu.edu

² Department of Astronomy, Yale University, New Haven, CT 06520

³ School of Physics, University of Melbourne, VIC 3010, Australia

⁴ University of Michigan, Department of Astronomy, 830 Denison Building, Ann Arbor, MI 48109-1042

⁵ Institute of Astronomy, School of Physics, University of Sydney, Australia

⁶ Research School of Astronomy and Astrophysics, Australian National University, Cotter Road, Weston Creek, ACT 2611, Australia

⁷ European Southern Observatory, Karl-Schwarzschild-Str. 2, 85748 Garching b. München, Germany

⁸ Australia Telescope National Facility, CSIRO, P.O. Box 76, Epping, NSW 1710, Australia

⁹ Observatories of the Carnegie Institute of Washington, Pasadena, CA, 91101

¹⁰ Space Telescope Science Institute, 3700 San Martin Drive, Baltimore, MD 21218

¹¹ Department of Astronomy, Columbia University, 550 West 120th Street, New York, NY 10027

¹² WIYN Consortium, Inc., 950 North Cherry Avenue, Tucson, AZ 85726

¹³ Department of Physics, University of Queensland, Brisbane, QLD 4072, Australia

¹⁴ Centre for Astrophysics and Supercomputing, Swinburne University of Technology, Mail 31, PO Box 218, Hawthorn, VIC 3122, Australia

¹⁵ School of Physics, University of Western Australia, Crawley, WA 6009, Australia

¹⁶ Institute of Astronomy, Madingley Road, Cambridge CB3 0HA, United Kingdom

¹⁷ Cerro Tololo Inter-American Observatory (CTIO), Casilla 603, La Serena, Chile

Neutral Gas Galaxies (SINGG), and the Survey of Ultraviolet emission in Neutral Gas Galaxies (SUNGG). $H\alpha$ emission traces the presence of ionizing O stars, which have initial masses $\mathcal{M}_* \gtrsim 20M_\odot$, while UV emission traces both O and B stars with $\mathcal{M}_* \gtrsim 3M_\odot$, giving the leverage in mass needed to probe the IMF.

The H I selection performed by SINGG and SUNGG results in a sample of star forming galaxies spanning the full range of morphologies seen in star forming galaxies with very few $H\alpha$ non-detections (Meurer et al. 2006, hereafter M06) and can fully account for the cosmic density of star formation in the local universe (Hanish et al. 2006, hereafter H06). By using this sample we avoid the issue of selection effects biasing towards particular extreme star formation histories (SFH) such as starburst galaxies. While the SFH of the universe as whole appears to have undergone a dramatic factor of 10 decline since $z \sim 1$ (~ 8 Gyr ago for $H_0 = 70 \text{ km s}^{-1} \text{ Mpc}^{-1}$ which we adopt here) this is still long compared to the lifetimes of the O ($\lesssim 7$ Myr) and B ($\lesssim 320$ Myr) stars probed in this study, so the SFH should be effectively constant for the sample as a whole.

There are a few other advantages of our approach. We use integrated fluxes, so in the parlance of Weidner & Kroupa (2005) we are dealing with the Integrated Galaxial IMF (IGIMF). Unlike the case of color-magnitude diagram analysis, crowding effects are irrelevant as are concerns as to the birth place of stars and their eventual dispersal in the field. Stochastic effects are minimized by integrating over whole galaxies, and the results are more comparable to studies of distant galaxies for which little more than total fluxes are available.

This paper is organized as follows. In Sec. 2 we discuss the sample selection, the data used, the measurements of these data which we make, and the necessary corrections to the measurements. In Sec. 3 we demonstrate the sensitivity of the measured fluxes to the IMF parameters and present a benchmark stellar population model for interpreting the results. Section 4 shows our primary result - that there is a strong correlation of the $H\alpha$ to UV flux ratio with surface brightness of both $H\alpha$ and R band emission, as well as weaker correlations of this ratio with other quantities. In Sec. 5 we discuss other physical parameters that can affect this ratio and argue that the IMF parameters are most likely driving the observed correlations. Section 6 places our results in the context other work, presents a physical scenario for pressure driven IMF variations driving the observed correlations, and discusses the implications of our results. Section 7 summarizes our results and suggests future observations.

2. OBSERVATIONS AND MEASUREMENTS

2.1. Sample Selection

Our sample consists of 103 galaxies with both $H\alpha$ observations from SINGG and UV observations from SUNGG. The ultimate parent of both these surveys is the H I Parkes All Sky Survey, HiPASS (Meyer et al. 2004; Koribalski et al. 2004). M06 discuss the selection of the SINGG sample in detail. In brief, the sample was selected uniformly in the log of H I mass, \mathcal{M}_{HI} , with the nearest galaxies preferred in order to yield the best spatial resolution. Only H I properties were used to select the SINGG sample. SUNGG is a Cycle 1 GALEX Legacy Survey, whose targets were all chosen from the SINGG sample (Wong 2007; Wong, et al. 2008). Because of the large GALEX field of view (1.1° diameter), some SINGG galaxies not in the original SUNGG selection are also

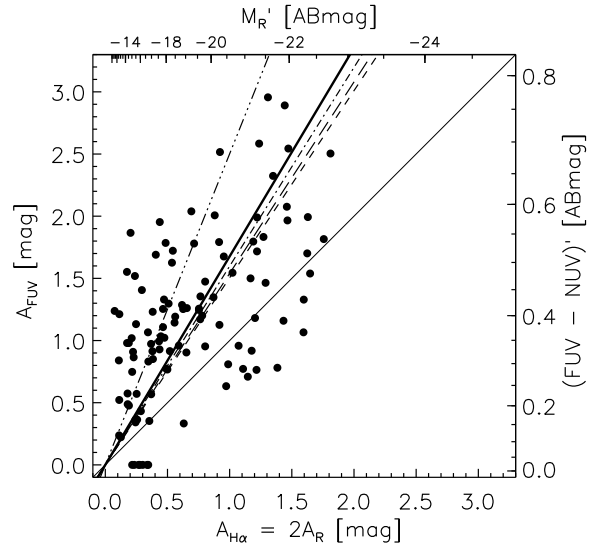


FIG. 1.— The adopted $H\alpha$ and FUV dust absorption in magnitudes, $A_{H\alpha}$ and A_{FUV} , respectively plotted against each other. These are determined from the R band absolute magnitude (M_R') and the FUV to NUV color $(FUV - NUV)'$ corrected for Galactic dust absorption but not internal dust absorption. These quantities are shown on the alternate axes (top and right, respectively). The thin solid line shows the unity relation ($A_{FUV} = A_{H\alpha}$). The heavy solid line shows the average ratio for our sample. The $A_{FUV}/A_{H\alpha}$ ratio expected for the (Calzetti, et al. 2000) and (Cardelli et al. 1989) dust absorption laws are shown with the long dashed and dash - triple dot lines, respectively; while the the ratio $A_{FUV}/(2A_{H\alpha})$ is shown by the short dashed and dash-dot lines respectively.

included in the measurements presented here. As shown by M06, HiPASS sources often correspond to multiple emission line galaxies (ELGs) in our narrow-band images (M06). By default we consider them part of the HiPASS source targeted. However, we have excluded five sources in multiple ELG fields from the analysis after inspecting the optical and UV images. Three of these are barely larger than the optical PSF and may be background galaxies (e.g. [O III] emitters at $z = 0.3$), one may be part of a larger galaxy and not a galaxy in its own right, and the last is not totally within the CCD frame.

2.2. Optical Observations

The $H\alpha$ and R band observations were obtained primarily with the CTIO 1.5m telescope, while some targets were observed with the CTIO 0.9m telescope to a similar depth, and at a similar plate scale. M06 describes the method of data acquisition, reduction and analysis. The data we use here are measurements of integrated flux and surface brightness. As detailed in M06 these are measured using concentric elliptical aperture photometry after masking out obvious foreground stars, background galaxies and other image blemishes from the sky subtracted images. Plots of enclosed flux as a function of aperture major axis radius are used to determine the total flux, F ; the radii enclosing 50% and 90% of the flux, r_{50} and r_{90} ; and the effective surface brightness Σ which is the face-on surface brightness within r_{50} : $\Sigma = F/(2\pi r_{50}^2)$, where here we use F to denote fluxes, or count rates in general. Later we become more specific and use F to denote integrated line fluxes and f to distinguish continuum flux density.

The $H\alpha$ signal to noise ratio is low, $S/N < 2$ within the outermost measurement aperture for 19 of the ELGs. In most of these $H\alpha$ is clearly detected, but its signal is washed out over the large apertures needed to measure the total flux. For these

cases we estimate the total $F_{\text{H}\alpha}$ as twice the $\text{H}\alpha$ flux within r_{50} determined from the R band. This correction factor is consistent with the observation that the $\text{H}\alpha$ and R emission typically have equal r_{50} values (H06). Since the measurement errors are much smaller within r_{50} this provides significant detections for 5 of the low S/N sources. We use upper limits based on the r_{50} extrapolated flux for the remaining 14 sources. Of these, only one, HIPASS J1321–31, has no $\text{H}\alpha$ emission discernible in our images. The optical counterpart is a Low Surface Brightness (LSB) galaxy identified using H I synthesis imaging observations presented by Ryan-Weber et al. (2003; also shown by Grossi et al. 2007). Pritzl et al. (2003) also note that no $\text{H}\alpha$ is seen in their WIYN 3.5m observations of J1321-31. This source is discussed further in Sec 5.4.

2.3. Ultraviolet Observations

The FUV and NUV GALEX images were typically 1500s (one eclipse) in duration, the same depth as the GALEX Nearby Galaxy Atlas (Gil de Paz et al. 2007). We make measurements from the combined flux calibrated images of each field taken from the GALEX pipeline (Morrissey et al. 2007). We perform our own background subtraction since the angular diameter of our galaxies is often $\gtrsim 3.2'$ which is the sky grid size used for GALEX pipeline processing (Morrissey et al. 2007). Fluxes, radii (r_{50} , r_{90}), and surface brightness in the FUV and NUV are measured in a manner analogous to that done for SINGG - using enclosed flux curves after masking out foreground and background objects.

The apertures used by SINGG and SUNGG are configured independently. Hence the UV and optical apertures generally are not matched, with the UV aperture almost always being larger. Comparison of the aperture areas with the r_{50} and r_{90} measurements, shows that the smaller of the UV or optical aperture should recover the majority of the flux at all wavelengths in almost all cases. Specifically, if the $\text{H}\alpha$ and UV light trace each other (as expected for a universal IMF) the bias induced by mismatched apertures in $\log(F_{\text{H}\alpha}/f_{\text{FUV}})$ should be ≤ 0.05 dex in 81% of the sample, may be as high as 0.3 dex in 17% and may be higher in 2% of the sample (2 cases). The actual bias depends on how much light is outside the optical measurement aperture, and may be considerably lower than these estimates if the IMF at large radii is deficient in high mass stars as found in some spiral galaxies (Thilker et al. 2005; Boissier et al. 2007).

2.4. Error bars

The error bars we display account for the measurement errors only. The errors in the optical quantities are discussed in detail in M06, and include terms for the sky uncertainty and the continuum subtraction. The errors in the UV quantities include terms for photon statistics and the background uncertainty (Wong 2007; Wong, et al. 2008).

2.5. Corrections for Emission Line contamination and Galactic Dust Absorption

A variety of corrections to the measurements are required to transform them to intrinsic quantities. M06 details the correction of the $\text{H}\alpha$ measurements for [NII] emission and Balmer absorption line contamination. The $\text{H}\alpha$, R , FUV, NUV measurements are all corrected for foreground Galactic dust absorption using the reddening maps of Schlegel et al. (1998) and the extinction law of Cardelli et al. (1989).

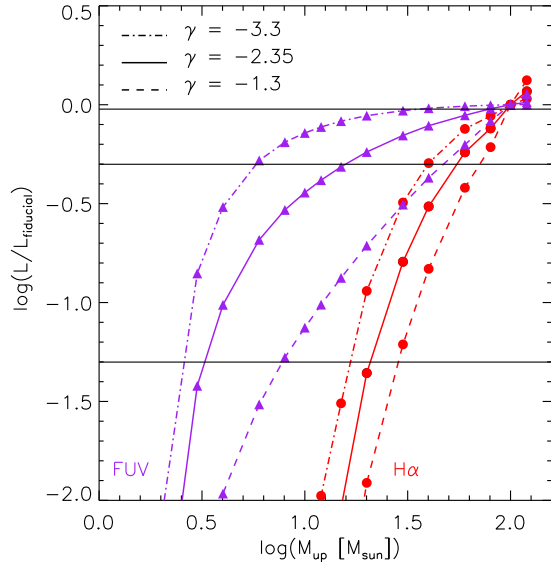


FIG. 2.— Sequences of population synthesis models showing the effects on the luminosity in $\text{H}\alpha$ and FUV of varying \mathcal{M}_u at fixed γ , relative to a fiducial model having $\mathcal{M}_u = 100 \mathcal{M}_\odot$. Three sequences corresponding to $\gamma = -3.3, -2.35, -1.3$ (differentiated by line style as shown in the legend) are shown for each band with the $\text{H}\alpha$ sequences shown as (red) connected dots and the FUV sequences as (purple) connected triangles. Horizontal lines from top to bottom indicate luminosities of 95%, 50%, and 5% relative to the fiducial model. See the text for further details of the models.

2.6. Correction for Internal Dust Absorption

Internal dust absorption can have a substantial effect on incident fluxes, especially in the UV, causing systematic biases in $F_{\text{H}\alpha}/f_{\text{FUV}}$. We correct the optical and UV data using separate empirical correlations.

For the UV data we base the correction on a fit to the correlation between the ratio of total far infrared (FIR) flux and the FUV flux and the FUV - NUV color. The total FIR flux was determined from IRAS fluxes following Dale et al. (2001) for 73 galaxies in the SUNGG sample that were detected by IRAS. The IRX- β data and fit for our sample is shown in Wong, et al. (2008). Similar correlations are shown by Cortese et al. (2006), Boissier et al. (2007), and Gil de Paz et al. (2007). The fitted relationship thus provides a method to recover the light absorbed by dust and re-radiated in the far-infrared.

The optical fluxes were corrected for internal dust using a relationship between $\text{H}\alpha$ dust attenuation derived from Balmer line ratios and R band absolute magnitude prior to internal dust correction, M'_R , found and presented by Helmboldt et al. (2004) using data from the Nearby Field Galaxy Survey (Jansen 2000; Jansen et al. 2000). The R band internal dust attenuation, in magnitudes was taken to be half that of $\text{H}\alpha$ to account for “differential” dust absorption: emission lines are more affected by dust than the stellar continuum (Fanelli et al. 1988; Calzetti, Kinney & Storchi-Bergman 1994), presumably because high-mass star formation is more highly correlated with dust than the general field star population. M06 present a population synthesis model attenuated by dust using this prescription in order to explain the relationship between L_R and the ratio of $\text{H}\alpha$ to FIR fluxes, $F_{\text{H}\alpha}/F_{\text{FIR}}$. The model used had a solar metallicity, a Salpeter IMF over the mass range of 0.1 to $100 \mathcal{M}_\odot$, and a constant SFR for a duration 100 Myr, and was calculated using Starburst99 (Leitherer et al. 1999),

TABLE 1
CONTRIBUTION TO LUMINOSITY BY STELLAR MASS

contribution level (1)	H α			FUV		
	$\gamma = -3.3$ (2)	$\gamma = -2.35$ (3)	$\gamma = -1.3$ (4)	$\gamma = -3.3$ (5)	$\gamma = -2.35$ (6)	$\gamma = -1.3$ (7)
5%	17	23	28	2.5	3.3	7.7
50%	40	54	71	5.7	16	47
95%	91	95	97	35	78	94

NOTE. — The values in this table correspond to the intersection of the horizontal lines with the curves shown in Fig. 2. They show the contribution of different stellar masses to the luminosity of a solar metallicity stellar population that has been forming stars for 1 Gyr. The stellar population has a single power law IMF with mass range of 0.1 to 100 M_{\odot} . The table gives the upper end of the mass range, in M_{\odot} , that contributes the first N% (specified in column 1) to the luminosity in H α (columns 2 - 4) and FUV (columns 5 - 7) for three different IMF slopes γ . Thus for a Salpeter IMF ($\gamma = -2.35$) 5%, 50%, and 95% of the H α luminosity comes from stars having masses up to 23 M_{\odot} , 54 M_{\odot} , and 95 M_{\odot} respectively, while 5%, 50%, and 95% of the FUV luminosity comes from stars having masses up to 3.3 M_{\odot} , 16 M_{\odot} , and 78 M_{\odot} respectively.

while the dust followed the Calzetti, et al. (2000) dust attenuation model. While this model accounted for the shape of the $F_{H\alpha}/F_{FIR}$ versus L_R relationship, there is an offset: $F_{H\alpha}/F_{FIR}$ is predicted to be too high by a factor of ~ 3 . There are various possible explanations for this discrepancy, some of which are discussed by M06. In particular, they note that adopting a steeper γ and/or lower \mathcal{M}_d will help alleviate the discrepancy. Hence, the low measured $F_{H\alpha}/F_{FIR}$ values may be related to the low $F_{H\alpha}/f_{FUV}$ values that are the primary concern of this investigation. Other possible factors that could contribute to the M06 $F_{H\alpha}/F_{FIR}$ model being too high include: too short of a duration for star formation, a metallicity that is too low, escaping ionizing photons, choice of stellar population models, a dust absorption model that is too differential, and an error in the FIR bolometric correction. It is beyond the scope of this paper to improve the $F_{H\alpha}/F_{FIR}$ versus M'_R model of M06. However, except for the dust bolometric correction, we do address all of these issues here with regard to our $F_{H\alpha}/f_{FUV}$ results. Since the overall shape of the $M'_R - F_{H\alpha}/F_{FIR}$ relationship agrees with the M06 model, then using this optical correction should yield the correct H α and R band fluxes modulo a zeropoint offset.

Figure 1 compares the internal dust absorption in the FUV, A_{FUV} , with that in H α , $A_{H\alpha}$, derived from the relations described above. It demonstrates that the internal dust corrections are broadly consistent with vectors from observed reddening laws, especially those that account for the differential extinction between emission lines and the stellar continuum (e.g. Calzetti, et al. 2000). Since these are transformations from the UV color and M'_R respectively, these quantities are shown on the alternate y and x axes. For our adopted dust absorption law, the x axis also shows $2A_R$ where A_R is the R band absorption. The Pearson correlation coefficient r_{xy} between A_{FUV} and $A_{H\alpha}$ is a 0.59. The probability to achieve this at random from uncorrelated quantities is 4×10^{-12} . The average ratio, $\langle A_{FUV}/A_{H\alpha} \rangle = 1.68$, is plotted as a thick solid line in Fig. 1. The dashed lines show that this is close to what is expected for the Calzetti, et al. (2000) starburst dust absorption model, which includes differential absorption, applied to population synthesis models (as described below). This model results in $A_{FUV}/A_{H\alpha} = 1.54$ and $A_{FUV}/(2A_R) = 1.50$. The observed average ratio is somewhat shallow for H α compared to “normal” dust reddening laws, where dust and gas are treated the same. For example, using the same modeling we calculate $A_{FUV}/A_{H\alpha} = 2.50$ for the Cardelli et al. (1989) reddening

law (shown as the dash - triple dot line in Fig. 1). A better agreement is found with the continuum, $A_{FUV}/(2A_R) = 1.60$ for Cardelli et al. (1989) (dash - dot line).

The amplitude of the dust corrections are also consistent with what is known about normal star forming galaxies. Our sample has a range of $A_{H\alpha}$ from 0.13 to 1.8 mag with an average and median of 0.71 and 0.56 mag respectively. We compare this to the Spitzer Infrared Nearby Galaxy Survey (SINGS) for which galaxy averaged $A_{H\alpha}$ can be estimated from a weighted average of H α and Spitzer 24 μ m fluxes, following the calibration presented by Calzetti et al. (2007). Kennicutt et al. (2008) do this and find the SINGS sample has $A_{H\alpha}$ ranging from 0 to 2.5 mag with the median at ~ 0.7 mag. That is, broadly consistent with what we find. For the FUV, we find A_{FUV} ranging from 0 to 3.03 mag, with an average and median of 1.2 mag. From Fig. 8 of Gil de Paz et al. (2007) it can be seen that A_{FUV} typically lies between 0.6 and 2 mag in their angular diameter selected sample. Despite the general consistency of our dust corrections with expectations, one must always be careful of the biases dust may cause, especially in cases like ours where the estimate of the correction is indirect. For example, Fig. 1 shows that relative to the $\langle A_{FUV}/A_{H\alpha} \rangle$ line, galaxies with low $A_{H\alpha}$ ($\lesssim 0.6$ mag) tend to have high A_{FUV} , while for high $A_{H\alpha}$ ($\gtrsim 1$ mag) A_{FUV} tends to be low compared to $A_{H\alpha}$. In Sec. 5.1 we show that this difference does not have a significant effect on our results.

2.7. Quantities and units

The primary quantity we work with here is the ratio of the H α line flux $F_{H\alpha}$, to the FUV flux density f_{FUV} (incident flux per unit wavelength), $F_{H\alpha}/f_{FUV}$, which has units of \AA . We compare this to the effective surface brightness in H α and the R band, $\Sigma_{H\alpha}$ and Σ_R , respectively. We show the H α surface brightness $\Sigma_{H\alpha}$ in units of W Kpc $^{-2}$ ($= 5.1 \times 10^{47} \text{ erg cm}^{-2} \text{ s}^{-1} \text{ arcsec}^{-2}$) and the R band surface brightness in units of $L_{R,\odot}$ Kpc $^{-2}$, where the sun’s R luminosity is $L_{R,\odot} = 4.39 \times 10^{22} \text{ W \AA}^{-1}$ ($M_{R,\odot} = 4.61 \text{ ABmag}$).

3. STELLAR POPULATION MODELS

3.1. Sensitivity to IMF parameters

The luminosity in H α and FUV of a stellar population arise from different but overlapping mass ranges of stars; this drives the sensitivity of $F_{H\alpha}/f_{FUV}$ to the properties of the upper end of the IMF. This is illustrated in Fig. 2 which shows the effect of varying \mathcal{M}_u on the expected H α and

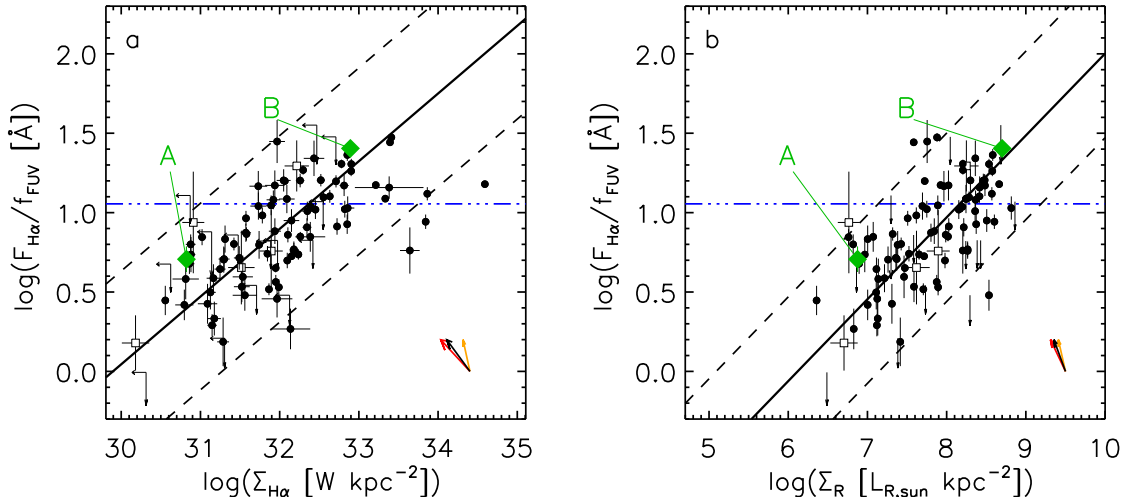


FIG. 3.— The ratio of $H\alpha$ line flux to FUV flux-density as a function of (a) the face-on $H\alpha$ effective surface brightness, and (b) (right) the face-on R band effective surface brightness Σ_R . All quantities have been corrected for Galactic and internal dust absorption as described in the text. The solid line shows the iteratively clipped least squares fit to the data, while the dashed lines show the final clipping limits. The dot-dash line shows the $F_{H\alpha}/f_{FUV}$ expected for our fiducial stellar population (eq. 3). The vectors in the lower right portion of the panels shows the effect of internal dust absorption according to the Calzetti, et al. (2000) starburst attenuation law (red vector) the Cardelli et al. (1989) Milky Way dust extinction law (orange vector), as well as our method (black vector). The length of the vectors in $\log(F_{H\alpha}/f_{FUV})$ in all cases is set to the average correction we deduce. Galaxies corresponding to measurements A and B are shown in Fig. 4.

FUV luminosities for stellar populations having a single slope IMF with $\mathcal{M}_l = 0.1 \mathcal{M}_\odot$, and a constant fixed SFR for the stars having $\mathcal{M}_* \leq 1 \mathcal{M}_\odot$. The stellar population synthesis models were calculated using the online Starburst99 package (v5.1, Leitherer et al. 1999; Vázquez & Leitherer 2005). They use solar metallicity Padova group evolutionary tracks (Bressan et al. 1993; Fagotto et al. 1994a,b; Girardi et al. 2000) and model atmospheres from Pauldrach et al. (2001) and Hillier & Miller (1998); these are the default options in Starburst99. Case B recombination was assumed to convert the output of ionizing photons to an $H\alpha$ luminosity (Osterbrock 1989). The FUV luminosity was determined by applying the GALEX FUV transmission curve to the spectra generated by Starburst99. We adopt a fixed duration $\Delta t = 1$ Gyr for the star formation so the births of O and B stars are in equilibrium with the deaths. Figure 2 shows that only stars with $\mathcal{M}_* \gtrsim 3 \mathcal{M}_\odot$ contribute significantly to the $H\alpha$ or FUV luminosities and these have main sequence lifetimes ≤ 325 Myr (Schaerer et al. 1993a,b; Fagotto et al. 1994a,b). Three model sequences with IMF slope $\gamma = -1.3, -2.35, -3.3$ are illustrated. The central value corresponds to the Salpeter (1955) slope which is consistent with more recent determinations of Kroupa (2001, 2002), while the other two values are meant to represent shallow and steep extremes to the slope. The y axis plots the luminosities relative to the case were $\mathcal{M}_u = 100 \mathcal{M}_\odot$. This corresponds to the highest stellar mass determined dynamically using binary star orbits (Bonanos et al. 2004; Rauw et al. 2004; Schnurr et al. 2008) and is a typical \mathcal{M}_u adopted in the literature. The horizontal lines indicate the masses below which the contribution to the luminosities is 5%, 50% and 95% of the total luminosity if the true \mathcal{M}_u is $100 \mathcal{M}_\odot$. We tabulate the \mathcal{M}_* values corresponding to these contributions in Table 1.

The $H\alpha$ curves are very steep and closely spaced together. This indicates that the mass range contributing to the $H\alpha$ luminosity is more sensitive to \mathcal{M}_u than γ . The opposite is true for the FUV luminosity - the curves are relatively shallow for \mathcal{M}_* near \mathcal{M}_u and the shapes are very different as a function of γ this indicates that the mass range contributing to the FUV

luminosity is more sensitive to γ than \mathcal{M}_u .

3.2. Fiducial stellar population model

From the models described above, we adopt the model with $\gamma = -2.35$ and $\mathcal{M}_u = 100 \mathcal{M}_\odot$ as our fiducial stellar population model. These parameters, or similar values are often used to characterize normal star forming stellar populations. For example Kennicutt (1998) adopted these parameters for his SFR calibrations, although they are based on different stellar population models (Madau, et al. 1998). From our fiducial model we derive the following SFR calibrations, and compare them to the Kennicutt (1998) calibrations (in parenthesis):

$$\frac{\text{SFR}(H\alpha)}{1 \mathcal{M}_\odot \text{ yr}^{-1}} = \frac{L_{H\alpha}}{1.04 (1.27) \times 10^{34} \text{ W}}, \quad (1)$$

$$\frac{\text{SFR}(FUV)}{1 \mathcal{M}_\odot \text{ yr}^{-1}} = \frac{l_{FUV}}{9.12 (9.09) \times 10^{32} \text{ W}^{-1}}. \quad (2)$$

Here the UV calibration of Kennicutt (1998) at $\lambda = 2150 \text{ \AA}$ was transformed to the pivot wavelength $\lambda_p = 1535 \text{ \AA}$ of the GALEX FUV filter assuming the an intrinsic power law FUV spectrum $f_\lambda \propto \lambda^\beta$ with UV spectral slope $\beta = -2$. To compare results to those that adopt the Kroupa (2001) IMF (e.g. Brinchmann et al. 2004; Kauffmann et al. 2003), the SFR estimates here should be divided by 1.5 (Brinchmann et al. 2004).

The ratio of eq. 2 and eq. 1 gives $F_{H\alpha}/f_{FUV}$ for the fiducial model:

$$\frac{F_{H\alpha}}{f_{FUV}} = 11.3 \quad (3)$$

We show this ratio in various plots as an indication of the a priori expected $F_{H\alpha}/f_{FUV}$.

In order to test the sensitivity of our results to the choice of stellar population models we also calculated models using the codes PEGASE (v2; Fioc & Rocca-Volmerange 1997, 1999) and GALAXEV (Bruzual & Charlot 2003). In both cases we adopted an IMF, metallicity, and SFH identical to the fiducial stellar population. Both the PEGASE and GALAXEV

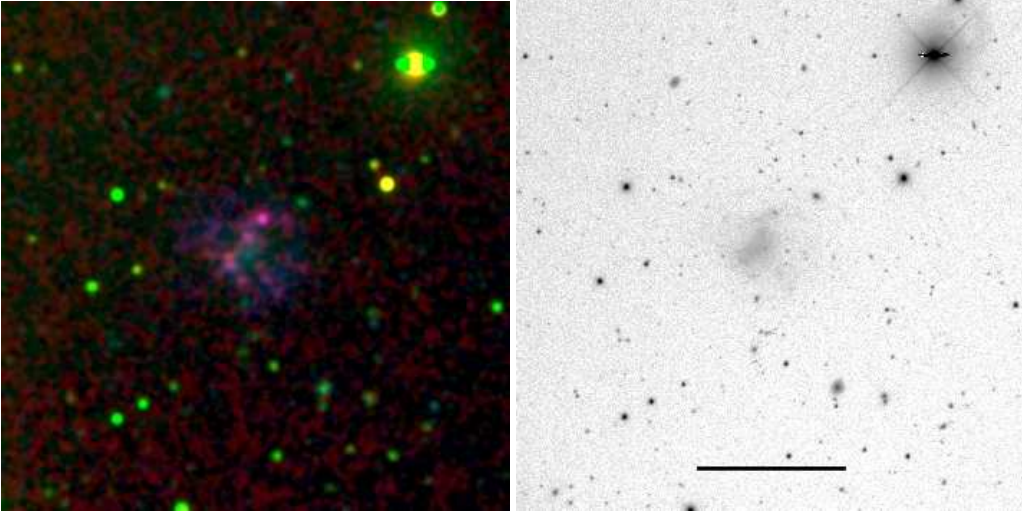


FIG. 4.— Example galaxy A - UGCA44 (HIPASS J0249–02) shown in $H\alpha$, R band, and FUV in red, green, and blue respectively in the left panel, while the right panel shows the R band only in an inverted gray scale. The three images that comprise the right panel have been convolved to have the GALEX resolution of $6.5''$, while the image on the left panel is shown at the original resolution of the SINGG data (typically $\sim 1.6''$). The scalebar in the right panel has a length of 10 Kpc.

TABLE 2
PROPERTIES OF EXAMPLE GALAXIES

Parameter	Example A	Example B	units
Name	UGCA044	NGC1566	
HIPASS+	J0249–02	J0419–54	
Morphology	IB(s)m:	(R')SAB(rs)bc	
$\log(\mathcal{M}_{\text{HI}})$	8.85	10.19	\mathcal{M}_{\odot}
$\log(L_R)$	8.29 ± 0.04	11.09 ± 0.01	$L_{R,\odot}$
M_{FUV}	-14.76 ± 0.04	-20.66 ± 0.00	ABmag
r_{50}	2.37 ± 0.05	6.76 ± 0.09	Kpc
$\log(\Sigma_{H\alpha})$	30.82 ± 0.07	32.89 ± 0.05	W Kpc^{-2}
$\log(\Sigma_R)$	6.87 ± 0.01	8.70 ± 0.01	$L_{R,\odot} \text{ Kpc}^{-2}$
$\log(F_{H\alpha}/f_{\text{FUV}})$	0.71 ± 0.08	1.40 ± 0.05	\AA

models use the same Padova group sources for their evolutionary tracks as does our Starburst99 model. The differences are in the Stellar atmospheres. The PEGASE model uses a library of observed stars (Fioc & Rocca-Volmerange 1997) while GALAXEV uses various BaSeL theoretical atmospheres as described by Bruzual & Charlot (2003). We used our own software to calculate f_{FUV} as described above, while the models provide either $L_{H\alpha}$ (PEGASE) or ionizing photon flux from which we calculate $L_{H\alpha}$ (GALAXEV). We calculate an equilibrium $F_{H\alpha}/f_{\text{FUV}} = 10.8, 11.8$ for the PEGASE and GALAXEV models respectively. Hence, differences in stellar population models can affect the $F_{H\alpha}/f_{\text{FUV}}$ calculations at the $\sim 10\%$ level. Metallicity also effects the model results; metallicity sensitivity is considered in Sec. 5.5.

The SFR conversion factors and equilibrium $F_{H\alpha}/f_{\text{FUV}}$ values all assume that the IMF is universal. However, as shown here, it is likely that the IMF is variable and often is not consistent with our fiducial model. Pflamm-Altenburg et al. (2007) examine the implications to $H\alpha$ based SFR estimates from an IGIMF that depends on the SFR, as one would expect for star formation dominated by clusters of finite mass. Then the conversion factors can vary from the above by orders of magnitude. This scenario is discussed further in Sec. 5.4 and Sec 6.3.

4. RESULTS

Figure 3 shows our primary result: a strong correlation between $F_{H\alpha}/f_{\text{FUV}}$ and surface brightness in both $H\alpha$ (panel a), and in the R band, Σ_R (panel b). One striking aspect of the Figure is that more than half the sample has $F_{H\alpha}/f_{\text{FUV}}$ below normal. Except for possibly one weak $H\alpha$ detection, and one galaxy with an upper limit to $F_{H\alpha}/f_{\text{FUV}}$, this includes all of the LSB galaxies having $\log(\Sigma_{H\alpha}) \leq 31.7$ or $\log(\Sigma_R) \leq 7.5$. Ordinary least squares bisector fits were performed to the data, with iterative clipping of the points having residuals outside of $\pm 2.5\sigma_y$ from the best fit line yielding

$$\log\left(\frac{F_{H\alpha}}{f_{\text{FUV}}}\right) = (-12.75 \pm 1.02) + (0.43 \pm 0.03) \log(\Sigma_{H\alpha}), \quad (4)$$

$$\log\left(\frac{F_{H\alpha}}{f_{\text{FUV}}}\right) = (-3.16 \pm 0.28) + (0.52 \pm 0.03) \log(\Sigma_R). \quad (5)$$

These are shown as solid lines in Fig. 3 while the clipping limits are shown as dashed lines. Data with only $H\alpha$ upper limits were not included in any of our fits. The quality of the correlations and fits are very similar with each having a Pearson's correlation coefficient $r_{xy} = 0.65$, a probability of $\sim 4 \times 10^{-12}$ that the correlation could have occurred from random data, and an rms dispersion of 0.22 dex about the $\log(F_{H\alpha}/f_{\text{FUV}})$ residuals (after clipping).

Optical surface brightnesses are not the only quantities that correlate with $F_{H\alpha}/f_{\text{FUV}}$. This is illustrated in two ways. First, in Fig. 4 we show example images of galaxies at either end of the correlations as indicated in Fig. 3; some properties of these two examples are given in Table 2. This illustrates the correlation with morphology along this sequence. The LSB example galaxy, UGCA44 is a dwarf irregular galaxy without coherent structure. The High Surface Brightness (HSB) example, NGC 1566, the brightest member of the Dorado group, is a strong regular two arm spiral galaxy. These two examples are typical of the morphological variation along the sequence, and consistent with what is known about the sequence of star forming galaxies: LSB sources are typically low luminosity irregular systems, HSB galaxies tend to be high luminosity spirals (as well as some blue compact dwarfs), galaxies with moderate surface brightness are a mixture of late type spirals and brighter irregulars.

Second, $F_{H\alpha}/f_{\text{FUV}}$ correlates with other global quantities such as total luminosity L_R and rotational velocity V_{rot} (determined from the H I line widths as outlined in H06), which is

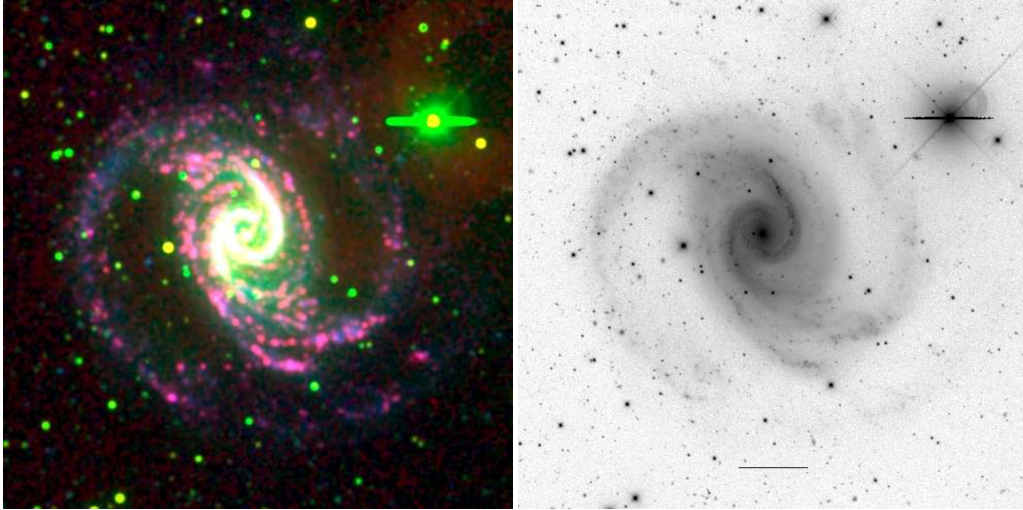


FIG. 4.— continued. Example galaxy B - NGC1566 (HiPASS J0419–54). The right and left panels have the same display levels as the other example. The projected area of these images is larger, while the scalebar length remains 10 Kpc.

shown in Fig. 5. Only HiPASS sources corresponding to single ELGs with optical axis ratio $a/b > 1.4$ are plotted in panel b, in order to limit the plot to galaxies likely to be dominated by rotation. Using the same fitting algorithm as described above, we find

$$\log\left(\frac{F_{\text{H}\alpha}}{f_{\text{FUV}}}\right) = (-1.64 \pm 0.15) + (0.27 \pm 0.01)\log(L_R), \quad (6)$$

$$\log\left(\frac{F_{\text{H}\alpha}}{f_{\text{FUV}}}\right) = (-0.97 \pm 0.17) + (0.96 \pm 0.09)\log(V_{\text{rot}}). \quad (7)$$

These correlations are weaker than those shown in Fig. 3, having correlation coefficients of 0.61 (0.57) while the (clipped) rms scatter in the $\log(F_{\text{H}\alpha}/f_{\text{FUV}})$ residuals is 0.19 (0.32) dex in panel a (b). Nevertheless, the probability that these correlations could have come from randomly drawn data is still low: 10^{-10} for the correlation with $\log(L_R)$, and 3×10^{-4} for the correlation with $\log(V_{\text{rot}})$ (low, but much higher than the other correlations shown here because of the smaller sample of elongated single ELGs).

The range of luminosity and mass in these correlations are too large for galaxies to evolve from one end of the correlation to the other. Instead, $F_{\text{H}\alpha}/f_{\text{FUV}}$ is one of the global properties (although not a fundamental one) that vary regularly along the sequence of late type galaxies. Other well known correlations along this sequence include the Hubble (1926) morphological sequence, the Tully-Fisher (1977) relation, the mass-metallicity relation (Tremonti et al. 2004) and the Universal Rotation Curve (Persic & Salucci 1991; Persic et al. 1996). The main physical parameter that drives most of these correlation appears to be halo-mass. However, the correlations in Fig. 3 are stronger than those in Fig. 5 indicating that star formation intensity and stellar mass density are more important for driving the $F_{\text{H}\alpha}/f_{\text{FUV}}$ correlations than halo properties.

Both the range of $F_{\text{H}\alpha}/f_{\text{FUV}}$ values, covering over a factor of ten, and the correlation with surface brightness have major implications, as discussed in Sec. 6.3.

5. PARAMETERS AFFECTING $F_{\text{H}\alpha}/f_{\text{FUV}}$

Physical properties that can affect $F_{\text{H}\alpha}/f_{\text{FUV}}$ include dust absorption, the detailed SFH, the porosity of the interstellar medium, stochastic effects from the number of stars, the metallicity of the stellar populations, and the properties of the IMF. We now consider, in turn, which of these could drive the observed correlations, saving the IMF for last because it is the only option we can not rule out.

5.1. Dust

The dust corrections are too small and in the wrong sense to have spuriously caused the observed correlations. Moreover, even without any dust corrections, a large fraction of the sample have too few ionizations for the observed UV light compared to expectations for normal star forming populations. These points are illustrated in Fig. 6 which is similar to Fig. 3, but here the quantities are shown before internal dust correction (and denoted with a prime: $\Sigma'_{\text{H}\alpha}$, Σ'_R and $F'_{\text{H}\alpha}/f'_{\text{FUV}}$). We see strong correlations between the quantities even before dust correction. Here $r_{xy} = 0.66$ (0.69) for the correlation between $F'_{\text{H}\alpha}/f'_{\text{FUV}}$ and $\Sigma'_{\text{H}\alpha}$ (Σ'_R), while the probability that these are spurious correlations from random data is 7×10^{-13} (3×10^{-14}). The best fits to these data are

$$\log\left(\frac{F'_{\text{H}\alpha}}{f'_{\text{FUV}}}\right) = (-11.32 \pm 1.14) + (0.39 \pm 0.04)\log(\Sigma'_{\text{H}\alpha}), \quad (8)$$

$$\log\left(\frac{F'_{\text{H}\alpha}}{f'_{\text{FUV}}}\right) = (-3.36 \pm 0.32) + (0.58 \pm 0.04)\log(\Sigma'_R). \quad (9)$$

As before, the fits are OLS bisector fits with an iterative 2.5σ clipping. The scatter about the fit is 0.22 (0.23) dex in $\log(F'_{\text{H}\alpha}/f'_{\text{FUV}})$ for the $\Sigma'_{\text{H}\alpha}$ (Σ'_R) data, nearly identical to the scatter seen in Fig. 3.

There are several reasons why reddening correction does not greatly effect the results. First, the average dust correction, shown by the black arrows in Figs. 3 and 6, is not large compared to the range of the correlations. Second, The difference in the dust correction between the high and low surface brightness ends is also not that large. This is shown by dividing the sample into quartiles of $F'_{\text{H}\alpha}/f'_{\text{FUV}}$. The quartile boundaries are at $\log(F'_{\text{H}\alpha}/f'_{\text{FUV}}) = 0.91, 1.04,$ and 1.26 and shown with dotted lines in Fig. 6. The average of the uncorrected points within the quartiles are shown as large pink triangles, while the average of the same data points after dust correction is shown with large cyan diamonds; thick lines show OLS-bisector fits to these average points. Systematic changes in the $A_{\text{FUV}}/A_{\text{H}\alpha}$ ratio noted in §2.6 are also not large enough to seriously effect the results.

Figure 6 also shows that nearly half the sample have $F_{\text{H}\alpha}/f_{\text{FUV}}$ below the value for our fiducial stellar population model. The first quartile has $\langle \log(F'_{\text{H}\alpha}/f'_{\text{FUV}}) \rangle = 0.73 \pm 0.10$, where here the error is the average error on $\log(F'_{\text{H}\alpha}/f'_{\text{FUV}})$. Hence, the galaxies in this quartile have $\log(F'_{\text{H}\alpha}/f'_{\text{FUV}})$ val-

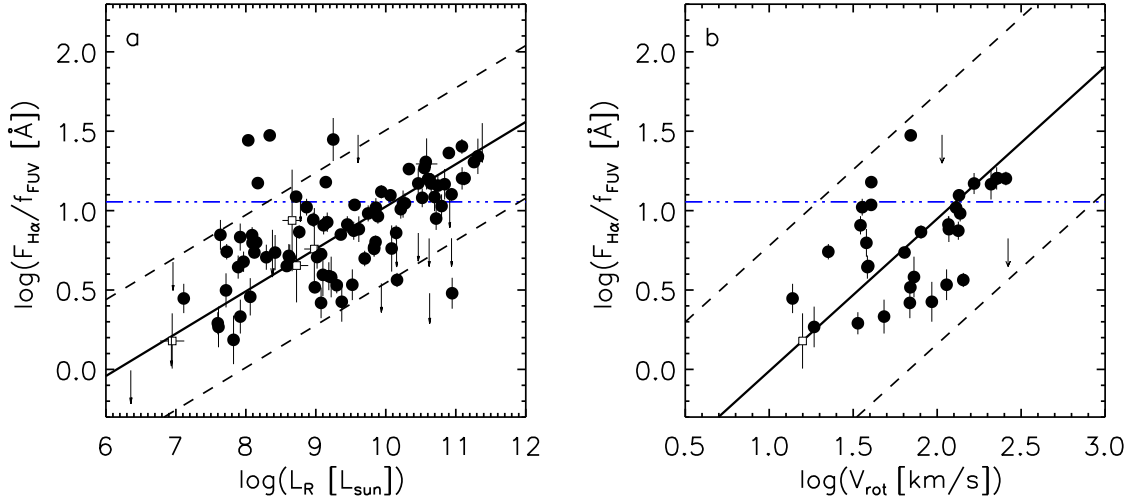


FIG. 5.— $F_{\text{H}\alpha}/f_{\text{FUV}}$ as a function of (a) R band luminosity and (b) rotational velocity. The symbol and line types have the same meaning as in Fig. 3.

ues that are on average 3σ lower than the fiducial model even before dust correction.

Could it be that we are *under* correcting for dust absorption? This seems unlikely, because the amount of dust needed to flatten the relationships shown in Fig. 3, is implausibly high and would only exacerbate the problem of low $F_{\text{H}\alpha}/f_{\text{FUV}}$ values. To flatten the relationship we consider the amount of dust required to bring the quartile $\langle \log(F'_{\text{H}\alpha}/f'_{\text{FUV}}) \rangle$ values equal to that of the first quartile. In other words, this assumes that the first quartile is virtually unaffected by dust. Since dust almost certainly effects all measurements this will produce an underestimate of the dust correction needed. In the second, third, and fourth quartiles $\langle \log(F'_{\text{H}\alpha}/f'_{\text{FUV}}) \rangle = 0.97, 1.15, 1.43$ respectively. Using $\langle A_{\text{FUV}}/A_{\text{H}\alpha} \rangle = 1.68$ (Sec. 2.6) then to lower these to the value observed in the first quartile requires $A_{\text{H}\alpha} = 0.9, 1.6,$ and 2.6 mag, respectively, and $A_{\text{FUV}} = 1.5, 2.6,$ and 4.4 mag, respectively. This is equivalent to an overall average $A_{\text{H}\alpha} = 1.3$ mag and $A_{\text{FUV}} = 2.1$ mag, or about twice the value estimated in Sec. 2.6.

Much of the scatter in the observed correlations may come from uncertainties in the internal dust correction. From the scatter in the IRX- β fits of Wong, et al. (2008) and Cortese et al. (2006) combined with the relationship between IRX and FUV dust absorption A_{FUV} of Buat et al. (2005) we determine that about 0.14 dex uncertainty in f_{FUV} results from the IRX- β relation. The correction to $F_{\text{H}\alpha}$ for dust absorption is tied to Balmer Decrement measurements. Kewley et al. (2002) show that after dust correction the SFR estimated from $\text{H}\alpha$ and FIR emission agree well in the calibrating Nearby Field Galaxy Sample. Using the online version of their table 1, we find a dispersion in their mean $\log(\text{SFR}_{\text{FIR}}/\text{SFR}_{\text{H}\alpha})$ of 0.16 dex (after an iterative 2.5σ clipping). Assuming this is the intrinsic scatter due to dust correction affecting $F_{\text{H}\alpha}$, and that it is uncorrelated with the scatter in f_{FUV} , then the uncertainty in $\log(F_{\text{H}\alpha}/f_{\text{FUV}})$ due to dust may be as high as 0.21 dex. This is very close to the observed scatter in Figures 3 and 5. However, this might be an overestimate of the scatter due to dust since $\text{SFR}_{\text{H}\alpha}$ estimates of Kewley et al. are also affected by the IMF.

Driver et al. (2007,2008) find strong inclination dependent differences in the luminosity functions of the bulge and disk components of galaxies which they attribute to dust absorption. While inclination effects may be seen in, and removed

from, the UV with our color based A_{FUV} estimate, our $A_{\text{H}\alpha}$ estimate is just based on luminosity and any inclination term should remain and effect or $F_{\text{H}\alpha}/f_{\text{FUV}}$ estimates. However, we found insignificant correlation coefficients $r_{xy} = 0.13, 0.01$ for the residuals of the fits in Fig. 3 panel (a) and (b), respectively, and the axial ratio (a/b) of the sources in the optical, demonstrating that inclination induced dust absorption is not significantly contributing to the scatter. Further work is required to determine what is causing the scatter in these relationships.

5.2. Star Formation History

Sharp changes in the SFR can strongly effect $F_{\text{H}\alpha}/f_{\text{FUV}}$ due to the different lifetimes of O and B stars. To explore the effects of a variable SFR on our correlation we built photometric models of a temporary increase, or “burst”, and decrease, or “gasp”, on an otherwise constant SFR population buildup. The models were created using Starburst 99 to calculate the evolution of the spectrum of a simple stellar population (i.e. instantaneous starburst). The evolution of the relevant luminosities ($\text{H}\alpha$, FUV and R) for an arbitrary SFR as a function of time, t , were calculated from the simple stellar population results using a separate program. These models employed the same fiducial IMF outlined in Sec. 3.2.

Figure 7 shows the burst and gasp SFHs that we modeled, the evolution of the fluxes $F_{\text{H}\alpha}$, f_{FUV} , and f_R , and the evolution of the ratio $F_{\text{H}\alpha}/f_{\text{FUV}}$. The models are relative in the sense that the absolute SFR is not important and is set by adding appropriate zeropoints. Hence the SFR and fluxes are shown relative to those before the burst or gasp. The functional form that we adopt is a constant SFR with a Gaussian enhancement or depression representing a burst and gasp, respectively. The model parameters are the FWHM duration, Δt , of the event, the ratio of maximum to minimum SFR, A , and the time t_0 of the center of the event. All models have a finite base SFR. We do not allow the SFR to completely turn-off because our sample shows that almost all late type galaxies have at least some recent high mass star formation (M06). For the burst models, the maximum SFR occurs during the event and the minimum is the base level, while for gasp models, the minimum SFR occurs during the event and the maximum is the base level. All models have $t_0 = 10$ Gyr. Absolute time is important when considering R band fluxes; our choice places

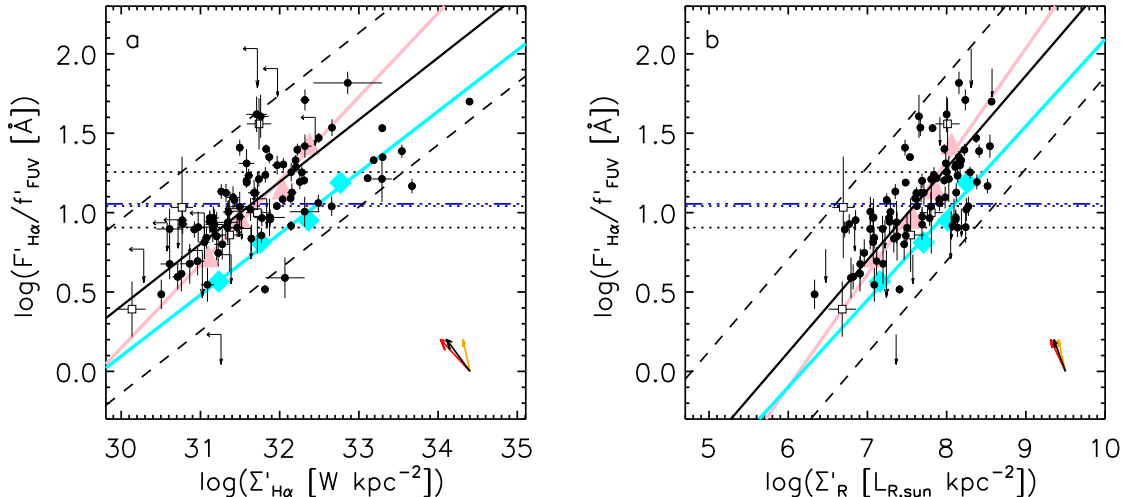


FIG. 6.— The quantities shown in Fig. 3 are plotted here prior to dust absorption correction, and hence are denoted with prime (') symbols. The dotted lines separate the sample into quartiles of $\log(F'_{\text{H}\alpha}/f'_{\text{FUV}})$. The pink triangles show the average quantities of the data points in each quartile, while the blue diamonds shows the average of the same points after dust correction. The thick pink and cyan lines are least squares fits to the respective average points. The meaning of the other symbols and lines are the same as in Fig. 3.

the burst or gasp at roughly the Hubble time.

We explored a range of model parameters and found that the salient features of these models can be illustrated with models having $\Delta t = 10, 100, 1000$ Myr, and $A = 2, 10, 100$. Figure 7 shows that very large excursions in $F_{\text{H}\alpha}/f_{\text{FUV}}$ are possible, especially for large A and short Δt . The $\Delta t = 1$ Gyr models produce only very weak excursions in $F_{\text{H}\alpha}/f_{\text{FUV}}$ because the timescale is long compared to the lifetimes of both the O and B stars.

Figure 8 plots the tracks the models make in the $F_{\text{H}\alpha}/f_{\text{FUV}}$ versus $\Sigma_{\text{H}\alpha}$ and Σ_R planes. All models converge at our adopted surface-brightness zeropoints and $\log(F_{\text{H}\alpha}/f_{\text{FUV}}) = 1.055$, the equilibrium value (eq. 3). We chose $\log(\Sigma_{\text{H}\alpha} [\text{W Kpc}^{-2}]) = 32.3$ and $\log(\Sigma_R [L_{R,\odot} \text{Kpc}^{-2}]) = 8.2$ as the zeropoints corresponding to the surface brightness immediately prior to the burst or gasp ($t = t_0 - 2\Delta t$) since these values are near the middle of the pack with respect to other galaxies having similar $F_{\text{H}\alpha}/f_{\text{FUV}}$. We also ran the models with the same IMF, metallicity and SFHs but based on PEGASE model calculations. Other than the zero-point offset noted in Sec. 3.2, these models make indistinguishable tracks from those shown in Fig. 8.

Both the burst and gasp models can produce large correlated excursions in $\Sigma_{\text{H}\alpha}$ and $F_{\text{H}\alpha}/f_{\text{FUV}}$ mimicking the observed correlations. This is especially true for the gasp models. However, in cases of large A and short Δt the tracks can enter unpopulated regions of the $F_{\text{H}\alpha}/f_{\text{FUV}}$ versus $\Sigma_{\text{H}\alpha}$ diagram during the post-burst phase as $F_{\text{H}\alpha}/f_{\text{FUV}}$ drops and $\Sigma_{\text{H}\alpha}$ fades to its original value. Fine tuning of the SFH to have a longer duration to the turn-off phase may alleviate this problem. The $F_{\text{H}\alpha}/f_{\text{FUV}}$ versus Σ_R plane is more difficult to explain with burst or gasp models. This is because short Δt events do not last long enough to significantly change Σ_R , while the long δt events that can cause large Σ_R excursions have little effect on $F_{\text{H}\alpha}/f_{\text{FUV}}$. Thus a SFH including a recent burst or gasp can not simultaneously account for the correlations of $F_{\text{H}\alpha}/f_{\text{FUV}}$ with both Σ_R and $\Sigma_{\text{H}\alpha}$. If bursts and gasps cause the spread of $F_{\text{H}\alpha}/f_{\text{FUV}}$ then the SFH of galaxies must be synchronized so that LSB galaxies would all be in a gasp or post-burst phase. We can think of no physical mechanism that can naturally result in such a contrived scenario.

While the burst and gasp models can produce large excursions in $F_{\text{H}\alpha}/f_{\text{FUV}}$, this requires short Δt and large A events. What amplitudes and durations are likely for intermittent star formation? Causality dictates that the event duration should not be shorter than the dynamical time, τ_{dyn} since it is the timescale for disturbances (such as the build-up or removal of ISM) to travel through a galaxy. Figure 9 displays the distribution of τ_{dyn} calculated from the H I profile width for the galaxies in our sample with axial ratio $a/b > 1.4$. These calculations follow the method of H06 for calculating V_{rot} H I line width and adopt $\tau_{\text{dyn}} = \tau_{\text{orb}}/\sqrt{3\pi}$, where $\tau_{\text{orb}} = 2\pi r_{50}/V_{\text{rot}}$. This definition effectively adopts a flat rotation curve which is evaluated at the $\text{H}\alpha$ r_{50} , and represents an average τ_{dyn} for high mass star formation in the galaxies. For rotation curves that are rising at r_{50} , this definition underestimates τ_{dyn} . From Fig 9 it can be seen that the median $\tau_{\text{dyn}} \approx 60$ Myr. Numerical simulations of starbursts indicate durations as low as ~ 60 Myr for the final sharp peak in the SFR during a merger, with the peak amplitudes on the order of 10-80 times the base level Mihos & Hernquist (1994a,b, 1996). These simulations show that enhanced star formation during a merger lasts several 100 Myr. Mergers are dramatic rare events and our sample shows very few examples of these ($< 10\%$, M06). Normal variations in SFR should be weaker and longer. For example, morphological and SED analyses of starbursting dwarf galaxies suggest $A \lesssim 3$ and Δt in the range of several 100 Myr (Meurer et al. 1992; Papaderos et al. 1996a,b; Marlowe et al. 1999). Our models indicate that such events may add scatter to our correlations but can not explain the large range in $F_{\text{H}\alpha}/f_{\text{FUV}}$.

5.3. Porosity of the Interstellar medium

The observed $F_{\text{H}\alpha}/f_{\text{FUV}}$ correlations could also occur if the escape fraction of ionizing photons, f_{esc} , inversely correlates with surface brightness. This explanation would require that the galaxies in the lowest quartile of $F_{\text{H}\alpha}/f_{\text{FUV}}$ are losing $\gtrsim 50\%$ of their ionizing flux compared to our fiducial model. Escaping ionizing photons have been detected in UV bright star forming galaxies at a redshift $z \sim 3$ (Steidel et al. 2001; Shapley et al. 2006; Iwata et al. 2008). In the local universe, direct measurements of f_{esc} have been limited to HSB star-

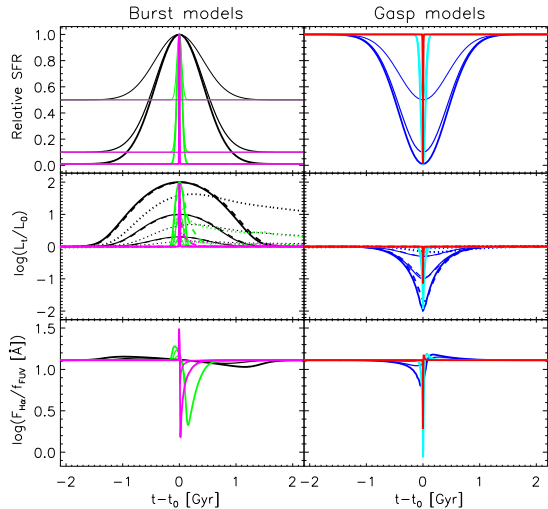


FIG. 7.— Models of the photometric evolution of “burst” and “gasp” SFHs are shown in the left and right panel respectively. The top panels show the relative star formation rate for the adopted Gaussian profile SFH. The x axis on all panels is the time relative to the event center t_0 . Three FWHM durations $\Delta t = 10, 100, 1000$ Myr are displayed using different colors: magenta, green, and black respectively for burst models; and red, cyan, and blue, respectively for gasp models. Three relative amplitudes, defined as SFR maximum:minimum are shown - 2:1, 10:1, 100:1 and distinguished with increasing line thickness. The color and thickness coding are repeated in the remaining panels and the next figure. The middle panel shows the evolution of luminosity relative to the pre-event luminosity (defined as $t_0 - 2\Delta t$) in the $H\alpha$, FUV, and R band distinguished using solid, dashed and dotted lines respectively. The bottom panels show the evolution $\log(F_{H\alpha}/f_{FUV})$.

burst galaxies and have mostly been upper limits in the range $f_{\text{esc}} < 0.05 - 0.1$ (Leitherer, et al. 1996; Hurwitz et al. 1997; Deharveng et al. 2001). The strongest claim for a direct detection of $f_{\text{esc}} \sim 0.04 - 0.11$ in Haro 11 by Bergvall et al. (2006) is disputed by Grimes et al. (2007) who find $f_{\text{esc}} \lesssim 0.02$ for the same data. The best case for escaping ionizing photons from a normal galaxy comes from the very faint $H\alpha$ emission detected in the Magellanic Stream and High Velocity Clouds which are thought to be partially ionized by the disk of our Galaxy (Bland-Hawthorn & Maloney 1999; Putman et al. 2003). These measurements require about 6% of ionizing photons to escape normal to the Galactic plane, or, about $f_{\text{esc}} \approx 1\% - 2\%$ when isotropitized over all angles. No direct measurements of f_{esc} from LSB galaxies have been attempted. Hence we can not directly rule out the possibility that f_{esc} inversely correlates with surface brightness.

However, there are two strong arguments against this notion. First, it implies the existence of “naked” O stars which we should see directly in HST images of the nearest low surface brightness galaxies. Instead, the color magnitude diagrams of dwarf irregulars are typically deficient in high mass stars (e.g. Tosi et al. 1991; Greggio et al. 1993; Marconi et al. 1995; Tolstoy 1996). While one may argue that the high mass stars are completely hidden by dust this would be inconsistent with them being naked. Furthermore, high mass stars can be isolated in large numbers from color-magnitude diagrams of higher surface-brightness dustier galaxies (e.g. Angeretti et al. 2005; Grochalski et al. 2008; Annibali et al. 2008). Second, this would require that dwarf LSB galaxies have an ISM that is more porous to ionizing photons than more massive galaxies. Dwarf galaxies with apparently porous H I distributions have been observed (e.g. HoII; Puche et al. 1992). However dwarf galaxies typically contain a higher fraction of their mass in the ISM (van Zee et al. 1995;

Swaters et al. 2002, H06) while the lower mass densities of their disks suggests that that the ISM distribution should be “puffier”. These factors should make it harder for ionizing photons to escape, not easier. Indeed, Using SINGG data (Oey et al. 2007) argue that f_{esc} increases with surface brightness. While we can not directly rule out a variable f_{esc} as driving the $F_{H\alpha}/f_{FUV}$ correlations we believe these arguments are sufficiently strong that a variable porosity scenario seems unlikely.

5.4. Stochastic limitations

Thilker, et al. (2007) and Boissier et al. (2007) use stochastic effects to explain the often seen strong UV emission beyond the $H\alpha$ truncation radius of spiral galaxies (Martin & Kennicutt 2001). They argue that the low $F_{H\alpha}/f_{FUV}$ results from stars forming in events that are too low in mass to have been likely to form O stars. In other words, the IMF is normal, but the star formation is too weak to produce the high mass stars. However, If the IMF is purely a statistical distribution of the masses of stars formed in a single event, then by averaging over many active star forming regions, one should recover the expected mean $F_{H\alpha}/f_{FUV}$ for the stellar population.

We find that the galaxies in our sample are all bright enough that they should have multiple O stars. We calculate this as follows. The minimum SFR needed to be likely to see a single O star is given by

$$\text{SFR}_{\min} = \frac{\langle \mathcal{M}_* \rangle N_*}{\langle \tau_O \rangle N_O} \quad (10)$$

where $\langle \mathcal{M}_* \rangle$ is the average star mass, $\langle \tau_O \rangle$ is the typical lifetime of an O star, and N_*/N_O is the ratio of the total number of stars and the stars formed above the O star mass limit for the chosen IMF. For a single power law IMF then

$$\langle \mathcal{M}_* \rangle = \left(\frac{\gamma+1}{\gamma+2} \right) \left(\frac{\mathcal{M}_u^{\gamma+2} - \mathcal{M}_l^{\gamma+2}}{\mathcal{M}_u^{\gamma+1} - \mathcal{M}_l^{\gamma+1}} \right) \quad (11)$$

and

$$\frac{N_*}{N_O} = \frac{\mathcal{M}_u^{\gamma+1} - \mathcal{M}_l^{\gamma+1}}{\mathcal{M}_u^{\gamma+1} - \mathcal{M}_O^{\gamma+1}}. \quad (12)$$

Where we adopt $\mathcal{M}_O = 20 \mathcal{M}_\odot$ as the minimum mass of an O star. For our fiducial IMF parameters (Sec 3.2) then $\langle \mathcal{M}_* \rangle = 0.35 \mathcal{M}_\odot$, $N_*/N_O = 1510$. Table 1 shows that for this IMF, and long duration star formation, the median mass contributing to $L_{H\alpha}$ is $\mathcal{M}_* = 54 \mathcal{M}_\odot$. We adopt the main sequence lifetime of such a star as $\langle \tau_O \rangle = 4.0$ Myr (Bressan et al. 1993), hence the SFR must exceed $\text{SFR}_{\min} = 1.3 \times 10^{-4} \mathcal{M}_\odot \text{year}^{-1}$ for it to be likely to observe one O star. This agrees very well with the simulations of Thilker, et al. (2007) showing that the “stochastic limit” for observing $H\alpha$ emission is at $\sim 10^{-4} \mathcal{M}_\odot \text{year}^{-1}$ for the same IMF parameters.

For our fiducial stellar population, we calculate that SFR_{\min} corresponds to $M_{FUV} = -8.29$ ABmag. This is a conservative estimate since shorter Δt would result in a fainter M_{FUV} . All the galaxies in our sample are significantly brighter than this, and we calculate that they should have $N_O \gtrsim 16$ for continuous star formation with the fiducial IMF. However, we note that HIPASS J1321-31 has a pre-dust extinction correction absolute magnitude of $M'_{FUV} = -9.61$, the faintest in our sample. This implies that we are only likely to see three or four O stars in this galaxy. This is the only source that looks like a complete $H\alpha$ non-detection in our sample. With this few O

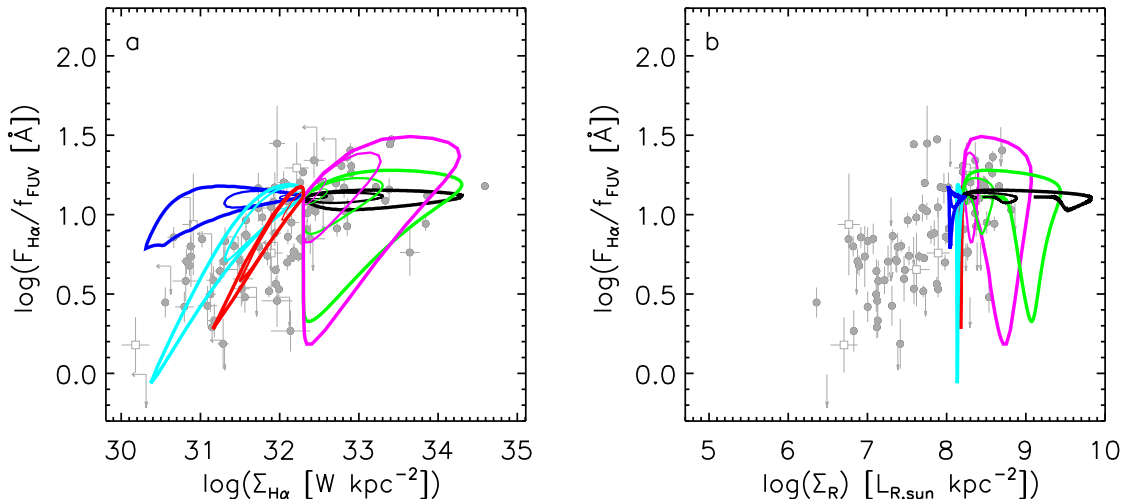


FIG. 8.— Tracks of $F_{H\alpha}/f_{FUV}$ versus $\Sigma_{H\alpha}$ (panel a) and Σ_R (panel b) made by the burst and gas SFHs shown in Fig. 7 using the same convention for line color to distinguish event duration and line thickness to represent event amplitude. The data is the same as in Fig. 3, but displayed in gray so the model lines show up clearly. The model trajectories converge on the pre-event values, for which we have adopted $\Sigma_{H\alpha}$ and Σ_R zero-points to be consistent with typical galaxies having the equilibrium $F_{H\alpha}/f_{FUV}$.

stars likely to be present at any one time, it could be that there is no $H\alpha$ because the dust absorption correction is overestimated and we caught the galaxy at “a bad time”. Otherwise, our target galaxies are well beyond the limit where statistical effects will bias $F_{H\alpha}/f_{FUV}$.

Stochastic effects may be even more important once plausible physical constraints are put on the IMF. Such an approach is adopted by Kroupa & Weidner (2003) and Weidner & Kroupa (2005) who consider the clustered nature of star formation, and impose the requirement that \mathcal{M}_u of a given cluster is statistically allowed for the mass of stars formed in the cluster $\mathcal{M}_{\text{cluster}}$. We refer to this as the cluster mass constrained IMF scenario. For an underlying $\gamma = -2.35$ (for the highest mass stars in a broken power law IMF following Kroupa 2001, 2002) this approach results in a strong correlation between \mathcal{M}_u and $\mathcal{M}_{\text{cluster}}$ for low masses ($\mathcal{M}_u \propto \mathcal{M}_{\text{cluster}}^{0.67}$) that asymptotes to the true stellar $\mathcal{M}_u \approx 150 M_{\odot}$ for clusters having $\mathcal{M}_{\text{cluster}} > 6800 M_{\odot}$ (Pflamm-Altenburg et al. 2007). For a power-law cluster mass function $\mathcal{M}_{\text{cluster}} \propto \mathcal{M}^{-2}$ the resultant IGIMF slope steepens to $\gamma \approx -2.8$ for the highest mass stars (Kroupa & Weidner 2003; Weidner & Kroupa 2005). The cluster mass constrained IMF scenario predicts that traditional $L_{H\alpha}$ to SFR conversion factors underestimate the true SFR, especially for $\text{SFR} < 10^{-2} M_{\odot} \text{ year}^{-1}$, up to two orders of magnitude higher than our estimate of SFR_{min} . The scenario can also account for the correlation between the luminosity of the brightest young star cluster and the SFR observed in galaxies Weidner et al. (2004). In a similar vein, Thilker, et al. (2007) also simulate the effects of requiring a certain mass of stars to form in each cluster before high mass stars can form, and find that such a prescription could result in an order of magnitude increase in the stochastic limit SFR_{min} . This could provide a reasonable explanation for the low $F_{H\alpha}/f_{FUV}$ values observed in LSB galaxies and outer disks. Indeed, Pflamm-Altenburg & Kroupa (2008) show the cluster mass constrained IMF scenario can produce $H\alpha$ edges and the non-linear relationship between the projected ISM density and $\Sigma_{H\alpha}$ observed within galaxies. Further implications of this scenario for our results are discussed in Sec. 6.3.

While the cluster mass constrained IMF scenario is based

on an IMF that has an invariant form, the resultant IGIMF is variable and only approaches this form for very high SFRs. Thus this can not be considered a constant IMF, but rather an explanation of what could cause the IGIMF to vary. Furthermore, while the scenario is appealing, the physical basis for it is somewhat elusive. It in essence is replacing a probabilistic interpretation of the IMF “the formation of a high mass stars in a low mass cluster is unlikely” with a deterministic interpretation “the formation of a high mass stars in a low mass cluster is impossible”. The implication is that \mathcal{M}_u is set by the available gas supply. However, the formalism is based on the final stellar mass of the cluster, not the gas mass of the progenitor. Forming or “embedded” clusters are found in molecular clouds having $M \geq 100 M_{\odot}$ (Lada & Lada 2003), sufficient to form at least one star with our adopted \mathcal{M}_u , so it is not the ISM supply that is limiting \mathcal{M}_u . In reality the molecular clouds fragment, and especially for low mass clusters, the star formation efficiency is low and the clusters do not remain bound (Lada & Lada 2003). So in effect, nature may produce stars in a way that resembles the cluster mass constrained IMF. In Sec. 6.2 we discuss an alternative scenario for a variable IMF based on the physics of high mass star formation.

5.5. Metallicity

Metallicity affects $F_{H\alpha}/f_{FUV}$ via line blanketing, which affects the stellar atmosphere temperatures. We calculated Starburst99 stellar population models with the same parameters as our fiducial population model but with metallicities of $Z = 0.004$ and 0.05 (1/5 and 2.5 times solar metallicity). These metallicities were used for both the isochrones and the spectra used to calculate the fluxes. These models result in $F_{H\alpha}/f_{FUV} = 14.0$ and 8.2 respectively. Decreasing metallicity increases $F_{H\alpha}/f_{FUV}$ as the hotter stellar atmospheres results in relatively more ionizing photons compared to the non-ionizing UV continuum. The models cover from SMC to super solar metallicities and result in a ~ 0.25 dex change in $F_{H\alpha}/f_{FUV}$, far smaller than the range of the $F_{H\alpha}/f_{FUV}$ variations. Since LSB dwarf galaxies typically have lower metallicities than normal galaxies, any trends with Σ should act to reduce the observed correlations, rather than contribute to

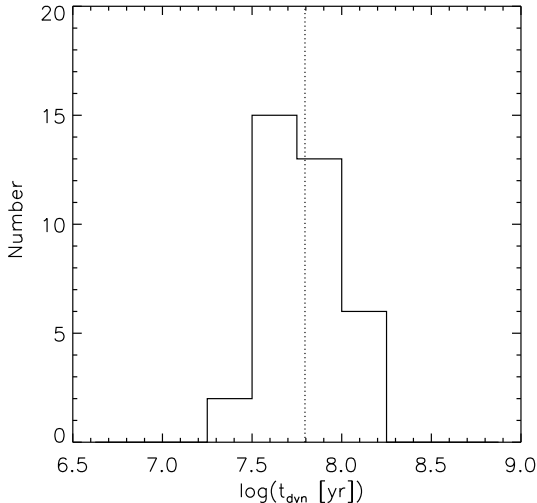


FIG. 9.— Distribution of dynamical times of the sample galaxies consisting of single ELGs having $a/b > 1.4$. The dotted line shows the median of the distribution.

them. Therefore, we conclude that metallicity does not contribute to the observed correlations of $F_{H\alpha}/f_{FUV}$ with surface brightness.

These results hold for equilibrium models with our fiducial IMF parameters. Further exploration of models having different parameters show that for very steep $\gamma \lesssim -3.3$ and $Z = 0.004$ $F_{H\alpha}/f_{FUV}$ becomes smaller than for solar metallicity models. This is shown in Fig. 10b discussed below. As metallicity decreases lower mass stars make a larger contribution to the FUV emission, and for very steep γ values this becomes more important than the increased output of ionizing photons.

5.6. IMF variations

Figure 10 show results of Starburst99 models designed to probe the sensitivity of $F_{H\alpha}/f_{FUV}$ to the IMF parameters \mathcal{M}_u and γ . The models have constant SFR over duration Δt up to 1 Gyr, and (mostly) solar metallicity. We hold other parameters fixed to the values of our fiducial stellar population model. In panel a. \mathcal{M}_u is varied and $\gamma = -2.35$ is held fixed, while in panel b. γ is varied and $\mathcal{M}_u = 100 \mathcal{M}_\odot$ is held fixed. In this panel we also explore cases with $Z = 0.004$ and $Z = 0.05$ and $\Delta t = 1$ Gyr in panel. Panel (c) shows the observed distribution of $F_{H\alpha}/f_{FUV}$ for comparison. We now consider whether the observed range of $F_{H\alpha}/f_{FUV}$ values can be modeled with long duration star formation by varying \mathcal{M}_u or γ . The full sample (excluding upper limits) spans $F_{H\alpha}/f_{FUV} = 1.5$ to 30\AA . Since the extremes may be affected by measurement errors, SFH variations, and stochastic effects we also consider the tenth to ninetieth percentile range of $F_{H\alpha}/f_{FUV}$ from 3 to 19\AA .

For a fixed (Salpeter) $\gamma = -2.35$ it is possible to reach the lowest $F_{H\alpha}/f_{FUV}$ with $\mathcal{M}_u \sim 20 \mathcal{M}_\odot$, and the tenth percentile with $\mathcal{M}_u = 30 \mathcal{M}_\odot$. With equilibrium star formation models ($\Delta t \gtrsim 300$ Myr) it is not possible to reach either the ninetieth percentile or maximum $F_{H\alpha}/f_{FUV}$ values. The maximum $\mathcal{M}_u = 120 \mathcal{M}_\odot$ allowed by the Starburst99 models results in an equilibrium $F_{H\alpha}/f_{FUV} = 12.9\text{\AA}$. The curves in Fig. 10a appear to be asymptotic towards high \mathcal{M}_u so it is unlikely that exploring higher \mathcal{M}_u would help. Lowering metallicity to $Z = 0.004$ brings the equilibrium $F_{H\alpha}/f_{FUV} = 14.0$ for $\mathcal{M}_u = 100 \mathcal{M}_\odot$ (Sec. 5.5) helping to alleviate the problem.

To achieve the highest observed $F_{H\alpha}/f_{FUV}$ values with solar metallicity and a Salpeter γ requires $\Delta t < 10$ Myr, shorter than the typical dynamical times of galaxies (Sec. 5.2), and thus rarely to be found in nature.

Varying γ can explain a much larger range of the observed $F_{H\alpha}/f_{FUV}$ values. Equilibrium star formation with $\gamma = -3.5$ can account for the lowest $F_{H\alpha}/f_{FUV}$ values, while the tenth percentile corresponds to $\gamma = -3.3$. The ninetieth percentile corresponds to $\gamma = -1.9$, while the maximum $F_{H\alpha}/f_{FUV}$ is slightly larger than the equilibrium $F_{H\alpha}/f_{FUV} = 26\text{\AA}$ for the shallowest $\gamma = -1.3$ we considered. For $Z = 0.004$ the maximum $F_{H\alpha}/f_{FUV}$ corresponds to $\gamma \approx -1.7$.

Having ruled out other possible explanations, we conclude that most of the observed range of $F_{H\alpha}/f_{FUV}$ values can most plausibly be explained as arising from long duration star formation with an IMF that varies at the upper end from galaxy to galaxy. The lowest observed values can occur by lowering \mathcal{M}_u to $\sim 30 \mathcal{M}_\odot$, steepening γ to ~ -3.3 or an intermediate combination of the two. It is harder to model the absolute highest observed $F_{H\alpha}/f_{FUV}$ values with equilibrium star formation at solar metallicity; lower metallicity can alleviate this problem.

6. DISCUSSION

6.1. Previous work

Ours is not the first study to probe the nature of the IMF using $H\alpha$ and UV observations, nor the first to claim evidence of IMF variations at the upper end. Buat, et al. (1987) used UV observations from the SCAP2000 experiment to explore the nature of the $H\alpha$ to UV flux ratio in a sample of bright spiral and irregular galaxies. They found a correlation in the ratio with morphological type, consistent to what we find: early type spirals have higher $F_{H\alpha}/f_{FUV}$ compared to late type spirals and irregulars. Technical issues (multiple instruments, uncertain dust corrections) limited them from making strong claims about the IMF. They also noted a varying f_{esc} could also explain their observed trend.

Recently, Hoversten & Glazebrook (2008) deduced variations of the upper end of the IMF using a very large ($\sim 140K$ galaxy) sample from the Sloan Digital Sky Survey (SDSS) and employing an $H\alpha$ equivalent width versus optical color diagram, following the method pioneered by Kennicutt (1983). They find that low luminosity galaxies have much lower $EW(H\alpha)$ than expected for their colors and argue that this is due to the upper end of the IMF varying systematically with galaxy mass. The variations are not monotonic with luminosity, but nevertheless similar to our results: low luminosity galaxies have less massive stars than higher luminosity galaxies. Their result is solid, but since optical bands are involved, much lower mass stars and longer timescales were required in their modeling to rule out other explanations.

Our contribution to the field is to return to the basic method of Buat, et al. (1987) with a larger sample and consistent dust absorption corrections. By using $H\alpha$ and FUV measurements we isolate the upper end of the IMF, and hence our constraints are more direct than $H\alpha$ – optical color comparisons. A new insight from our work is that the surface brightness, or more likely surface mass density, seems to be more important for driving the IMF variations than luminosity or mass as suggested by Hoversten & Glazebrook (2008). Our use of use of H I selection and measurement of $H\alpha$ and UV images results in an extended range of optical surface brightness compared to SDSS (M06), allowing this finding, while our inclusive sam-

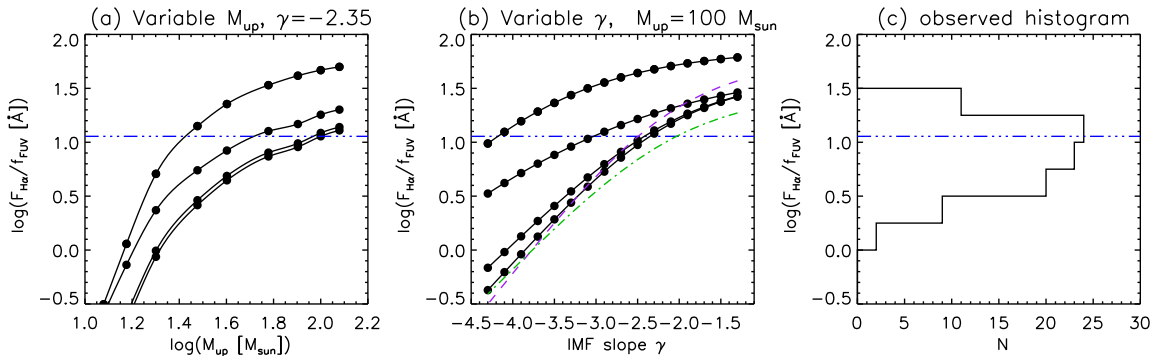


FIG. 10.— Starburst 99 model predictions of $F_{\text{H}\alpha}/f_{\text{FUV}}$ for stellar populations forming at a constant star formation rate are shown in panels (a) and (b). Panel (c) shows the distribution of observed $F_{\text{H}\alpha}/f_{\text{FUV}}$ values for comparison. In panel (a) the IMF slope γ is held constant at the Salpeter (1955) value while \mathcal{M}_u is varied. In panel (b) the upper mass limit is held constant at $\mathcal{M}_u = 100 \mathcal{M}_{\odot}$ while γ is varied. In these panels the dots indicate the \mathcal{M}_u and γ values used in the solar-metallicity ($Z = 0.02$) models, while solid lines connect the models for star formation durations of 0, 10 Myr, 100 Myr, and 1 Gyr (from top to bottom). The dashed (purple) and dot-dashed (green) lines in panel (b) indicate tracks with a metallicity $Z = 0.004$ and 0.05 respectively and a duration of 1 Gyr. The broken horizontal line in all panels shows the expected $F_{\text{H}\alpha}/f_{\text{FUV}}$ for our fiducial stellar population model (eq. 3).

ple selection eliminates the possibility that our results stem from a non-representative sample.

6.2. A scenario for the observed correlations

The belief that the form of the IMF is universal is largely based on observations of star clusters. Kroupa (2001) showed that apparent variations in γ observed in young star clusters could result purely from stochastic effects due to the limited number of massive stars. A universal IMF is then a logical conclusion if all stars form in star clusters as argued by Lada & Lada (2003).

Recent work suggests that this paradigm should be re-examined. Theory and simulations indicate that the highest mass stars ($> 10 \mathcal{M}_{\odot}$) require a dense cluster environment to form efficiently. It is hard to form these stars by simple collapse and fragmentation - the stars “turn on” and stop forming before high masses can be assembled. One way around this is by the process of competitive accretion whereby young proto-stars “steal” material from each others envelopes as well as accreting it from the dense ISM at the bottom of a cluster’s potential well (Bonnell, et al. 2004). This allows rapid assembly of massive stars but requires very dense environments, like star clusters, and especially their dense centers (Bonnell, et al. 2004). While all stars may form in clusters, not all clusters are alike. Clusters with a wide range of densities are known many of which are unbound (Lada & Lada 2003). Ephemeral unbound clusters are not likely to maintain a high enough density for long enough to have the collisions necessary to form the most massive stars.

Pressure plays a key role in regulating the phases of the ISM (McKee & Ostriker 1977; Wolfire et al. 2003; Blitz & Rosolowsky 2006), and is the most likely physical property for driving the observed $F_{\text{H}\alpha}/f_{\text{FUV}}$ correlations. While the neutral phases (cold and warm) are in pressure equilibrium with each other, the molecular ISM is self gravitating and supported by turbulence from star formation feedback (Dopita & Sutherland 2003). Blitz & Rosolowsky (2006) show that the ratio of molecular to neutral ISM in galaxies has a nearly linear relationship with the mid-plane pressure, P_{mid} , expected from hydrostatic equilibrium of a thin gas layer embedded in stellar disk with a significantly larger scale height. This leads to the expectation that

$$P_{\text{mid}} \propto \Sigma_{\star}^{0.5} \Sigma_{\text{g}} (\sigma_{\text{g}} / \sqrt{h_{\star}}), \quad (13)$$

where Σ_{\star} is the stellar mass density in the disk, Σ_{g} is the ISM mass density, σ_{g} is the ISM velocity dispersion, and h_{\star} is the

stellar scale height. The terms in parenthesis are not expected to vary much within galaxies nor from galaxy to galaxy. Σ_{\star} varies strongly between galaxies and to first order is $\propto \Sigma_{\text{R}}$. The molecular to neutral mass ratio in the ISM, and therefore the fraction of the ISM available for star formation, should be highly dependent on Σ_{R} , because it effectively is tracing pressure.

Elmegreen & Efremov (1997) and Elmegreen (2008b) show that tight bound clusters, and hence O stars, should preferentially form in a high pressure environment while at lower pressures unbound and loose clusters form (with less O stars). While the pressure they are referring to is that internal to the molecular clouds, P_{mid} provides a floor to this pressure and thus should have some bearing on the final internal pressures (Dopita & Sutherland 2003). By this reasoning, Σ_{R} traces P_{mid} which determines the likelihood that clusters are formed bound, thus regulating the O/B ratio and therefore $F_{\text{H}\alpha}/f_{\text{FUV}}$.

The link between compact cluster formation and surface brightness is well established observationally. Larsen & Richtler (2000) and Larsen (2004) used ground based and HST images of spiral galaxies to show that the fraction of U band light in star clusters correlates with the surface brightness of the host. Similarly, Billet et al. (2002) show that the fraction of U band light in star clusters scales almost linearly with Σ_{SFR} . Meurer et al. (1995) used Hubble Space Telescope NUV images to show that there is a correlation between fraction of NUV light in the form of star clusters and underlying surface brightness in starburst galaxies. While the correlation is weaker than that shown by Larsen (2004), the surface brightness range is smaller, with the starbursts corresponding to the high intensity, high cluster fraction extension of the sequence of Larsen.

Internal variations in $F_{\text{H}\alpha}/f_{\text{FUV}}$ within a galaxy may also be related to pressure variations. For example, M83 shows a sharp decline in its $F_{\text{H}\alpha}/f_{\text{FUV}}$ ratio (Thilker et al. 2005) corresponding to the $\text{H}\alpha$ truncation radius identified by Martin & Kennicutt (2001). The FUV surface brightness profile continues well beyond this radius, with no apparent sign of a truncation. Similar results are found in a larger sample by Boissier et al. (2007) showing that H II edges, generally are not seen in the FUV. Martin & Kennicutt (2001) show that the H II edges corresponds well to where Σ_{g} drops below the critical density needed for disk self-gravity (Martin & Kennicutt 2001). When a disk becomes gravitationally unstable it first

excites low order modes: bars and spiral arms. These will induce spiral shocks which will increase the ISM pressure and thus facilitate the formation of star clusters and the efficient formation of O stars. Thus star-formation edges may be a byproduct of the sharp-pressure increase associated with spiral arms in massive unstable disks.

Our scenario is somewhat complementary to the more mathematically developed cluster mass constrained IMF scenario of Kroupa and Weidner discussed in Sec. 5.4. Indeed, they could be compatible to the extent that our scenario offers a physical basis for small unbound clusters having a truncated IMF.

6.3. Implications of a variable top end of the IMF

If the upper end of the IMF is not uniform then there are several important astrophysical implications. First, the star formation rate (SFR) estimated for a galaxy depends on the tracer used. While $H\alpha$ and UV based SFR may agree for the bright galaxies, $H\alpha$ based SFRs will underestimate the contribution of LSB galaxies to the cosmic star formation density of the universe. Even if an alternate explanation of the $F_{H\alpha}/f_{FUV}$ variations were found (e.g. f_{esc} variations), SFR estimates will still be under-estimated from $H\alpha$ fluxes in LSB galaxies. Optically selected surveys of star formation will have results that depend on their surface brightness selection limits. Perhaps little notice has been paid to the problem of low $F_{H\alpha}/f_{FUV}$ values because most star formation surveys have concentrated on normal and HSB galaxies where the ratio is closer to normal. UV based SFR estimates should be more secure than $H\alpha$ estimates. However, there is no guarantee that IMF variations stop at the O - B star divide. For the cluster mass constrained IMF scenario Pflamm-Altenburg et al. (2007) show that when the SFR is very low ($SFR < 10^{-3} \mathcal{M}_{\odot} \text{yr}^{-1}$) that the IGIMF deviates from the canonical IMF down to \mathcal{M}_{*} of just a few \mathcal{M}_{\odot} and that standard conversion factors between $L_{H\alpha}$ and SFR could underestimate the SFR by orders of magnitude in such cases. However, at the low mass end, below $\sim 0.8 \mathcal{M}_{\odot}$, the IMF appears to be constant (Feltzing et al. 1999; Wyse et al. 2002). More work needs to be done to determine where between the masses of O stars and the sub-solar range that the IMF switches from being variable to constant.

Second, a varying IMF also implies that the feedback of the young stellar populations onto the ISM in terms of energy output and the return of chemically enriched material will also vary, with LSB galaxies having less feedback of energy and mass per mass in stars formed. The metallicity of the returned ISM will also be affected. LSB galaxies will have a lower [O/Fe] ratio and higher [N/O] ratio than normal or HSB galaxies. While such abundance anomalies are observed in LSB dwarf galaxies (e.g. Tautvaišienė et al. 2007) the abundance patterns are usually explained by galactic winds that preferentially expel oxygen rich ejecta in galaxies with weak gravitational potentials (Pilyugin 1992, 1993; De Young & Heckman 1994; Mac Low & Ferrara 1999; D’Ercole & Brighenti 1999). Undoubtedly such winds occur (e.g. NGC 1569: Waller 1991; NGC 1705: Meurer et al. 1992), but they would be harder to produce in a LSB dwarf compared to a HSB blue compact dwarf. Instead of removing excess metal content in a galactic wind, LSB galaxies may just not produce the metals. Recently, Köppen et al. (2007) were able to model the functional form of the mass-metallicity and mass yield relations of (Tremonti et al. 2004) using a cluster mass constrained IMF model described above (Sec 5.4) effectively demonstrating

this scenario is plausible.

Measurements of the SFH of nearby galaxies from color magnitude diagrams (CMDs) can also be misinterpreted. In such an analysis, one typically assumes that stars form with a Salpeter IMF fully populated up to $\sim 100 \mathcal{M}_{\odot}$. If \mathcal{M}_{u} is lower, or γ steeper than assumed, then one could spuriously infer recently truncated or declining SFHs. Indeed many galaxies in the nearby universe show very few field high mass stars. These include LSB dwarf irregulars (e.g. Tosi et al. 1991; Greggio et al. 1993; Tolstoy 1996), but also some blue compact dwarfs (Greggio et al. 1998; Cannon et al. 2003). The CMD results can then be interpreted as a SFH that is “gasping” (Marconi et al. 1995) or being in a “post-burst” phase (Cannon et al. 2003). Gasping could also result from a bias inherent in the star formation scenario: stars are harder to identify in crowded clusters, hence there is a bias against finding stars with life times shorter than the dissolution time of clusters (Marconi et al. 1995). However, there are also cases where the gasping deduced from CMDs is consistent with weak $H\alpha$ measurements (Tolstoy 1996; Cole et al. 2007). Claims based on CMD analysis that star formation is “contracting” or progressively halting from large radius to an inner starburst (e.g. Skillman et al. 2003) may also be cast in doubt if there is a radial variation of the IMF.

7. SUMMARY

We have looked at correlations of the integrated $H\alpha$ to far UV flux ratio $F_{H\alpha}/f_{FUV}$ with other global parameters in a sample of galaxies that well represents the full range of star formation properties of galaxies in the local universe. There are strong correlations of $F_{H\alpha}/f_{FUV}$ with optical surface brightness in both $H\alpha$ and the R band. Weaker but significant correlations are found with R band luminosity, rotational amplitude as well as morphology. Thus the systematic variations of $F_{H\alpha}/f_{FUV}$ are part of the family of observational galaxy scaling relations, such as the Hubble sequence, the Tully-Fisher relation, the mass-metallicity relation, the luminosity-surface brightness relation and the star formation law. However, unlike other scaling relations, the $F_{H\alpha}/f_{FUV}$ correlations appear to be more closely related to high mass star formation intensity or stellar mass density than halo mass.

We examined a variety of plausible explanations for the root causes of these correlations and ruled most of them out as follows. 1. While dust correction decreases $F_{H\alpha}/f_{FUV}$, the effect is not large enough to have spuriously created the correlations, and can not fix the problem of low $F_{H\alpha}/f_{FUV}$ values which exists even before dust correction. 2. Recent variations in the SFR would need to have had large amplitudes (factor $\gtrsim 10$) and short duration ($\lesssim 100$ Myr) to account for the range of $F_{H\alpha}/f_{FUV}$. The normal undisturbed morphology of the majority of our sample belie such extreme events in their recent histories. Furthermore, variations in the SFR can not account for the correlations of $F_{H\alpha}/f_{FUV}$ with both $\Sigma_{H\alpha}$ and Σ_R . Invoking SFH to explain the low $F_{H\alpha}/f_{FUV}$ in LSB galaxies would require all LSB galaxies to be experiencing coordinated gasps in their SFR which violates the Copernican principle. 3. Low $F_{H\alpha}/f_{FUV}$ values can occur if ionizing photons escape. However, one would then expect to see naked O stars in Hubble Space Telescope images of the nearest LSB galaxies, and typically they are not found. Furthermore, LSB galaxies tend to have a higher gas fraction, and should have thicker disks than normal galaxies which argues against them having a higher f_{esc} . 4. Stochastic effects can not cause the observed trends since we are measuring over entire galaxies, and they all are

sufficiently luminous in the UV, even without dust correction, that they should contain multiple O stars. The related cluster mass constrained IMF scenario of Kroupa & Weidner (2003) and Weidner & Kroupa (2005) may explain the results, but in effect it does not describe a constant IMF but a variable one. 5. Metallicity has only a fairly small effect on $F_{H\alpha}/f_{FUV}$ with lower metallicity acting to increase $F_{H\alpha}/f_{FUV}$ for a normal IMF. This is also in the wrong sense since LSB galaxies tend to have low metallicity and low $F_{H\alpha}/f_{FUV}$.

This leaves the most plausible explanation of the results to be a varying upper end of the IMF. The observed range $F_{H\alpha}/f_{FUV}$ can be explained if the upper mass limit M_u varies between 30 and 120 M_{\odot} , or the IMF slope γ varies between -1.3 and -3.3 . There is not enough information to decide between these options or rule out variations in both parameters.

We sketch a scenario that can explain the observed correlations as arising from the pressure regulated formation of tightly bound star clusters. These are the sites of the formation of the highest mass stars. A steeper or truncated IMF occurs when stars form in loose or unbound clusters. Regions of high pressure favor the formation of bound clusters resulting in an increased O/B star ratio and thus higher $F_{H\alpha}/f_{FUV}$. R band surface brightness traces pressures since it is the established stellar populations that dominate the disk potential and hence determines the mid-plane pressure at hydrostatic equilibrium.

There are several major implications of these results. The SFR estimated from $H\alpha$ and FUV measurements are not necessarily the same. This holds even if the correlations result from a variable f_{esc} instead of IMF variations. If the IMF is to blame, then the return of energy, momentum, and metals to the ISM from high mass stars is decreased in LSB galaxies. This provides an alternative driver for the mass metallicity relation other than galactic winds. Allowing IMF variations makes the interpretations of Color-Magnitude Diagrams difficult: an observed lack of high mass stars may be due to a truncated IMF rather than being due to a recent decrease in

the star formation rate. Hence interpretation of CMD results showing gasping/post-burst SFHs or radial truncations of star formation are cast in to doubt.

Further work is required to pin-down the nature of the $F_{H\alpha}/f_{FUV}$ variations. We are currently examining internal $F_{H\alpha}/f_{FUV}$ variations within our sample galaxies in order to determine the extent to which the IMF variations are local. More observations of LSB galaxies are needed to firmly rule out a variable f_{esc} as the cause of the variations. If LSB galaxies do have a high f_{esc} this would imply that either their H II regions no longer follow case B ionization, or that they have many naked O stars. Spectroscopic tests for either scenario should be possible. Careful CMD analyses, including UV measurements, of HSB and LSB galaxies can be used to determine how far down the IMF the variations may occur. Comparison of abundance ratios with surface brightness may provide constraints on the relative importance of a truncated IMF and starburst winds for determining the abundance patterns in dwarf galaxies.

Primary support for the work presented here was obtained through NASA Galex Guest Investigator grant GALEXGI04-0105-0009 and NASA LTSA grant NAG5-13083 to G.R. Meurer. Additional support in the early phase of the SINGG project came through grants NASA grants NAG5-8279 (Astrophysical Data Products program), HST-GO-08201, and HST-GO-08113 to G.R. Meurer. This work benefited from useful discussions with Rob Kennicutt, Evan Skillman, Chris Flynn, and Guinnevere Kauffmann as well as constructive comments from the anonymous referee. Some of the first analysis work for this project occurred while G.R. Meurer was visiting Germany in September 2007; he thanks his hosts in Munich - Sandra Savaglio and Uta Grothkopf, and in Freising - Ruth Lang and Armin Müller, for their hospitality.

Facilities: GALEX, CTIO:1.5m, CTIO:0.9m

REFERENCES

- Annibali, F., Aliosi, A., Mack, J., Tosi, M., van der Marel, R., Angeretti, L., Leitherer, C. & Sirianni, M. 2008, AJ, 135, 1900
- Angeretti, L., Tosi, M., Greggio, L., Sabbi, E., Aliosi, A., & Leitherer, C. 2005, AJ, 129, 2203
- Bergvall, N., Zackrisson, E., Andersson, B.-G., Arnberg, D., Masegosa, J., & Östlin, G. 2006, A&A, 448, 513
- Billet, O.H., Hunter, D.A., & Elmegreen, B.G. 2002, AJ, 123, 1454
- Bland-Hawthorn, J., & Maloney, P.R. 1999, ApJ, 510, L33
- Blitz, L., & Rosolowsky, E. 2006, ApJ, 650, 933
- Boissier, S. et al. 2007, ApJS, 173, 524
- Bonanos, A.Z., et al. 2004, ApJ, 611, L33
- Bonnell, I.A., Vine, S.G., & Bate M.R. 2004, MNRAS, 349, 735
- Bressan, A., Fagotto, F., Bertelli, G., & Chiosi, C. 1993, A&AS, 100, 647
- Brinchmann, J., Charlot, S., White, S.D.M., Tremonti, C., Kauffmann, G., Heckman, T., & Brinkmann, J. 2004, MNRAS, 351, 1151
- Bruzual, G., & Charlot, S. 2003, MNRAS, 344, 1000
- Buat, V., Donas, J., & Deharveng, J.M. 1987, A&A, 185, 33
- Buat, V., et al. 2005, ApJ, 619, L51.
- Calzetti, D., Armus, L., Bohlin, R.C., Kinney, A.L., Korneef, J., & Storchi-Bergmann, T. 2000, ApJ, 533, 682
- Calzetti, D., Kinney, A.L., & Storchi-Bergmann, T. 1994 ApJ, 429, 582
- Calzetti, D., et al. 2007, ApJ, 666, 870
- Cannon, J.M., Dohm-Palmer, R.C., Skillman, E.D., Bomans, D.J., Côté, S., & Miller, B. 2003, AJ, 126, 2806
- Cardelli, J.A., Clayton, G.C., & Mathis, J.S. 1989, ApJ, 345, 245
- Cole, A.A., et al. 2007, ApJ, 659, L17
- Cortese, L., et al. 2006, ApJ, 637, 242
- Dale, D.A., Helou, G., Contursi, A., Silberman, N.A., & Kolhatkur, S. 2001, ApJ, 549, 21
- Deharveng, J.-M., Buat, V., Le Brun, V., Milliard, B. Kunth, D., Shull, J.M., & Gry, C. 2001, A&A, 375, 805
- D’Ercole, A., & Brighenti, F., 1999, MNRAS, 309, 941
- De Young, D.S., & Heckman, T.M. 1994, ApJ, 431, 598
- Dopita, M.A., & Sutherland, R.S. 2003, “Astrophysics of the Diffuse Universe”, (Berlin: Springer)
- Driver, S.P., Popescu, C.C., Tuffs, R.J., Liske, J., Graham, A.W., Allen, P.D., & De Propriis, R. 2007, MNRAS, 379, 1022
- Driver, S.P., Popescu, C.C., Tuffs, R.J., Graham, A.W., Allen, Liske, J., & Baldry, I. 2008, ApJ, 678, L101
- Elmegreen, B.G., & Efremov, Y.N., 1997, ApJ, 480, 235
- Elmegreen, B.G. 2008a, in proceedings from “The Evolving ISM in the Milky Way and Nearby Galaxies: Recycling in the Nearby Universe”, arXiv:0803.3154
- Elmegreen, B.G. 2008b, ApJ, 672, 1006
- Fagotto, F., Bressan, A., Bertelli, G., & Chiosi, C. 1994a, A&AS, 104, 365
- Fagotto, F., Bressan, A., Bertelli, G., & Chiosi, C. 1994b, A&AS, 105, 29
- Fanelli, M.N., O’Connell, R.W., & Thuan, T.X. 1988, ApJ, 334, 665
- Feltzing, S., Gilmore, G., & Wyse, R.F.G. 1999, ApJ, 516, L17
- Fioc, M., & Rocca-Volmerange, B. 1997, A&A, 326, 950
- Fioc, M., & Rocca-Volmerange, B. 1999, astro-ph/9912179
- Gil de Paz, A. et al. 2007, ApJS, 173, 185
- Gilmore, G. 2000 in “Starburst Galaxies: Near and Far”, eds., L. Tacconi, D. Lutz (Berlin: Springer), p. 34
- Girardi, L., Bressan, A., Bertelli, G., & Chiosi, C. 2000, A&AS, 141, 371
- Greggio, L., Marconi, G., Tosi, M., & Focardi, P. 1993, AJ, 105, 894
- Greggio, L., Tosi, M., Clampin, M. De Marchi, G., Leitherer, C., Nota, A., Sirianni, M. 1998, ApJ, 504, 725
- Grimes, J.P., et al. 2007, ApJ, 668, 891.
- Grochalski, et al. M. 2008, ApJ, 686, L79.
- Grossi, M., Disney, M.J., Pritzl, B.J., Knezek, P.M., Gallagher, J.S., Minchin, R.F., & Freeman, K.C. 2007, MNRAS, 374, 107
- Hanish, D.J., et al. 2006, ApJ, 549, 150 (H06)

- Helmboldt, J.F., Walterbos, R.A.M., Bothun, G.D., O'Neil, K., & de Blok, W.J.G. 2004, *ApJ*, 613, 914
- Hillier, D.J., & Miller, D.L. 1998, *ApJ*, 496, 407
- Hoversten, E.A., & Glazebrook, K. 2008, *ApJ*, 675, 173
- Hubble, E.P. 1926, *ApJ*, 64, 321
- Jansen, R.A. 2000, Ph.D. thesis, Kapteyn Astronomical Institute, Univ. Groningen
- Jansen, R.A., Fabricant, D., Franx, M., Caldwell, N. 2000, *ApJS*, 126, 331
- Hurwitz, M., Jelinsky, P., & Dixon, W.V.D. 1997, *ApJ*, 481, L31.
- Iwata, I., et al. 2008, *ApJ*, submitted, (arXiv:0805.4012)
- Kennicutt, R.C. 1983, *ApJ*, 272, 54
- Kennicutt, R.C. 1998, *ARA&A*, 36, 189
- Kennicutt, R.C. 2008, *ApJ*, submitted
- Kewley, L.J., Geller, M.J., Jansen, R.A. & Dopita, M.A. 2002, *AJ*, 124, 3135
- Köppen, J., Weidner, C., & Kroupa, P. 2007, *MNRAS*, 375, 673
- Kroupa, P. 2001, *MNRAS*, 322, 231
- Kroupa, P. 2002, *Science*, 295, 82
- Kroupa, P. & Weidner, C. 2003, *ApJ*, 598, 1076
- Koribalski, B. et al. 2004, *AJ*, 128, 16
- Lada, C.J., & Lada, E.A. 2003, *ARA&A*, 41, 57
- Larsen, S.S., & Richtler, T. 2000, *A&A*, 354, 836
- Larsen, S.S. 2004, *A&A*, 416, 537
- Leitherer, C., Ferguson, H.C., Heckman, T.M., & Lowenthal, J.D. 1996, *ApJ*, 454, L19.
- Kauffmann, G., et al. 2003, *MNRAS*, 341, 54
- Leitherer, C. et al., 1999, *ApJS*, 123, 3
- Mac Low, M.-M., & Ferrara, A. 1999, *ApJ*, 513, 142
- Madau, P., Pozzetti, L., & Dickinson, M. 1998, *ApJ*, 498, 106
- Marconi, G., Tosi, M., Greggio, L., & Foccardi, P. 1995, *AJ*, 109, 173
- Marlowe, A.T., Meurer, G.R., & Heckman, T.M. 1999, *ApJ*, 522, 183
- Martin, C.L., & Kennicutt, R.C. 2001, *ApJ*, 555, 301
- McKee, C.F., & Ostriker, J.P. 1977, *ApJ*, 218, 148
- Meurer, G.R., Freeman, K.C., Dopita, M.A., & Cacciari, C. 1992, *AJ*, 103, 60
- Meurer, G.R., Heckman, T.M., Leitherer, C., Kinney, A., Robert, C., & Garnett, D.R. 1995 *AJ*, 110, 2665
- Meurer, G.R., et al. 2006, *ApJS*, 165, 307 (M06)
- Mihos, J.C., & Hernquist, L. 1994, *ApJ*, 425, L13
- Mihos, J.C., & Hernquist, L. 1994, *ApJ*, 431, L9
- Mihos, J.C., & Hernquist, L. 1996, *ApJ*, 464, 641
- Meyer, M.J., et al. 2004, *MNRAS*, 350, 1195
- Morrissey, P., et al., 2007, *ApJS*, 173, 682
- Oey, S.M., et al., 2003, *ApJ*, 661, 801
- Osterbrock, D.E. 1989, *Astrophysics of Gaseous Nebulae & Active Galactic Nuclei*, Mill Valley CA: University Science Books
- Papaderos, P., Loose, H.-H., Thuan, T.X., & Fricke, K.J. 1996, *A&AS*, 120, 207
- Papaderos, P., Loose, H.-H., Fricke, K.J., & Thuan, T.X. 1996, *A&A*, 314, 59
- Pauldrach, A.W.A., Hoffmann, T.L., & Lennon, M. 2001, *A&A*, 375, 161
- Persic, M. & Salucci, P., 1991, *ApJ*, 368, 60
- Persic, M. Salucci, P., & Stel, F. 1996, *MNRAS*, 281, 27
- Pflamm-Altenburg, J., Weidner, C., & Kroupa, P. 2007, *ApJ*, 671, 1550
- Pflamm-Altenburg, J., & Kroupa, P. 2008, *Nature*, 455, 641
- Pilyugin, L.S. 1992, *A&A*, 260, 58
- Pilyugin, L.S. 1993, *A&A*, 277, 42
- Pritzl, B.J., Knezek, P.M., Gallagher, J.S., Grossi, M., Disney, M.J., Minchin, R.F., Freeman, K.C., Tolstoy, E., & Saha, A. 2003, *ApJ*, 596, L47
- Puche, D., Westpfahl, D., Brinks, E., & Roy, J.-R. 1992, *AJ*, 103, 1841
- Putman, M.E., Bland-Hawthorn, J., Veilleux, S., Gibson, B.K., Freeman, K.C., & Maloney, P.R. 2003, *ApJ*, 597, 948
- Rauw, G., et al. 2004, *A&A*, 420, L9
- Ryan-Weber, E., Webster, R.L., & Staveley-Smith, L. 2003, *MNRAS*, 343, 1195
- Salpeter, E.E. 1955, *ApJ*, 121, 161
- Schaerer, D., Meynet, G., Maeder, A., & Schaller, G. 1993a, *A&AS*, 98, 523
- Schaerer, D., Charbonnel, C., Meynet, G., Maeder, A., & Schaller, G. 1993b, *A&AS*, 102, 339
- Schlegel, D.J., Finkbeiner, D.P., & Davis, M. 1998, *ApJ*, 500, 525
- Schnurr, O., Cassoli, J. Chené, A.-N., Moffat, A.F.J., St-Louis, N. 2008, *MNRAS*, 389, 38
- Shapley, A.E., Steidel, C.C., Pettini, M., Adelberger, K.L., & Erb, D.K. 2006, *ApJ*, 651, 688
- Skillman, E., Tolstoy, E., Cole, A.A., Dolphin, A.E., Abhijit, Gallagher, J.S., Dohm-Palmer, R.C., & Mateo, M. 2003, *ApJ*, 596, 253
- Steidel, C.C., Pettini, M., & Adelberger, K.L. 2001, *ApJ*, 546, 665
- Swaters, R.A., van Albada, T.S., van der Hulst, J.M., & Sancisi, R. 2002, *A&A*, 390, 829
- Tautvaišienė, G., Geisler, D., Wallerstein, G., Borissova, D., Pagel, B.E.J., Charbonnel, C., & Smith, V. 2007, *AJ*, 134, 2318
- Thilker, D.A., et al. 2005, *ApJ*, 619, L79-L82
- Thilker, D.A., et al. 2007, *ApJS*, 173, 578
- Tolstoy, E. 1996, *ApJ*, 461, 684
- Tosi, M., Greggio, L., Marconi, G., & Focardi, P. 1991, *AJ*, 102, 951
- Tremonti, C.A., et al. 2004, *ApJ*, 613, 898
- Tully, R.B., & Fisher, J.R. 1977, *A&A*, 54, 661
- van Zee, L., Haynes, M.P., & Giovanelli, R. 1995, *AJ*, 109, 990
- Vázquez, G.A., & Leitherer, C. 2005, *ApJ*, 621, 695
- Waller, W.H. 1991, *ApJ*, 370, 144
- Weidner, C., Kroupa, P., & Larsen, S.S. 2005, *MNRAS*, 350, 1503
- Weidner, C. & Kroupa, P. 2005, *ApJ*, 625, 724
- Wolfire, M.G., McKee, C.F., Hollenbach, D., & Tielens, A.G.G.M. 2003, *ApJ*, 587, 278
- Wong, O.I. 2007, PhD Thesis, University of Melbourne
- Wong, O.I. et al. 2008, in preparation.
- Wyse, R.F.G., Gilmore, G., Houdashelt, M.L., Feltzing, S., Hebb, L., Gallagher, J.S., & Smecker-Hane, T.A. 2002, *New A*, 7, 395